CEBAF Program Advisory Committee Six (PAC6) Proposal Cover Sheet

This proposal must be received by close of business on April 5, 1993 at:

CEBAF

User Liaison Office

12000 Jefferson Avenue

Newport News, VA 23606

Proposal Title

DEUTERON PHOTODISINTEGRATION BY LINEAR POLARIZED PHOTONS

Contact Person

Name: V. B. GANENKO

Institution: KHARKOV INST. OF PHYSICS & TECHNOLOGY

Address: AKADEMICHESKAJA ST, 1,

Address:

City, State ZIP/Country: KHARKOV, 310108 UKRAINE

Phone: (057) 235-1993 **FAX:** (057) 235-1738

E-Mail → BITnet: KFTI.KHARKOV.UN@RELAY.USSR.EU.NET **Internet:**

If this proposal is based on a previously submitted proposal or letter-of-intent, give the number, title and date:

PR 91-012

CEBAF Use Only

Receipt Date: 4/5/93 Log Number Assigned: PR 93-004

By: gp

CEBAF Program Advisory Committee Six (PAC6) Proposal Cover Sheet

This proposal must be received by close of business on April 5, 1993 at:

CEBAF
User Liaison Office
12000 Jefferson Avenue
Newport News, VA 23606

Proposal Title

Deuteron photodisintegration by linearly polarized photons

Contact Person

Name: V.B.Ganenko
Institution: Kharkov Institute of Physics & Technology
Address: Akademicheskaja St.,1,Kharkov,310108,Ukraine
Address:
City,State ZIP/Country:Kharkov, Ukraine
Phone: (057)-235-1993
FAX: (057)-235-1738
E-Mail→BITnet:kfti% kfti.kharkov.ua@ relay.ussr.eu.net
Internet:

If this proposal is based on a previously submitted proposal or letter-of-intent, give the number, title and date:

Proposal:PR-91-012
$\vec{\gamma}d \rightarrow pn$ Reaction Asymmetry Cross-Section Measurements

CEBAF Use Only

Receipt Date:
Log Number Assigned:
By:

RESEARCH PROPOSAL FOR CEBAF PAC6

Deuteron photodisintegration by linear polarized photons

K.A.Aniol[1], E.Brash[8], E.Cisbani[5], C.C.Chang[11], M.B.Epstein[1], J.M.Finn[3], S.Frullani[5], V.B.Ganenko[6] (Spokesperson), F.Garibaldi[5], F.Ghio[5], Shalev Gilad[7], R.Gilman[2,8], (Spokesperson), C.Glashausser[8], M.Jodice[5], L.Ya.Kolesnikov[6], A.S.Kostromin[6], G.Kumbartzki[8], R.De Leo[4] G.J.Lolos[12], R.Lourie[13], P.Markovitz[11], Z.Meziani[10], J.Mougey[9], S.Nanda[2], R.Perrino[4], R.Ransome[8], A.L.Rubashkin[6] P.Rutt[3], A.Saha[2], P.V.Sorokin[6] (Spokesperson), P.E.Ulmer[2], G.M.Urciuoli[5], Yu.V.Zhebrovskij[6]

[1]The California State University at Los Angeles
[2]The Continuous Electron Beam Accelerator Facility
[3]The College of William and Mary in Virginia
[4]INFN Sezione Lecce
[5]INFN Sezione Sanita, Rome
[6]Kharkov Institute of Physics and Technology
[7]Massachusetts Institute of Technology
[8]Rutgers University
[9]Saclay
[10]Stanford University
[11]The University of Maryland
[12]The University of Regina
[13]The University of Virginia, Charlottesville

Deuteron photodisintegration by linearly polarized photons

Abstract

We propose to measure the asymmetry of the $\gamma d \to pn$ cross section in the photon energy range $E_\gamma = 0.6 \to 2.4$ GeV. The measurements will be carried out with a linearly polarized photon beam, which is obtained by coherent bremsstrahlung of relativistic electrons in a diamond crystal. These measurements will allow one :

- to check the predictions of the available theoretical models of the $\gamma d \to pn$ process in the energy range of $1 \to 2$ GeV;

- to clarify whether quark mechanisms or hadron mechanisms determine $\gamma d \to pn$ in this energy range;

-to determine the possible addition of nonnucleon (N^*) configurations in the deuteron wave function and their characteristics;

- to check, using new experimental data, the phenomenon of asymptotic scaling in $\gamma d \to pn$ predicted in [3 - 6] and observed in SLAC experiments [1, 2].

The experiment will be a part of the program for studying $\gamma d \to pn$ proposed for CEBAF [7, 8].

Introduction

For more than fifty years deuteron photodisintegration

$$\gamma d \to pn \tag{1}$$

has attracted great deal of attention, since it is the simplest nuclear process whose studying allows one to check fundamental ideas of nuclear and elementary particle physics.

At the present time the photon energy range $E_\gamma \geq 1$ GeV is the most interesting for studying. In this range the reaction mechanisms are complicated and, apparently, substantially evolve with increasing energy. Resent measurements performed at SLAC [1, 2] show that at energies $E_\gamma \geq 1.4$ GeV mechanisms of the reaction caused by quark configurations are possible. At the same time according to theoretical computations [9] the data of ref. [1, 2] can be satisfactory described within the framework of the meson – nucleon theory up to the energy $E_\gamma \approx 2$ GeV. At higher energy ($E_\gamma \approx 2.4$ GeV) a change in the reaction mechanism is possible, and the description of the process using QCD may be more adequate.

One should expect that qualitatively new information on the process (1) in the range of energy higher than 1 GeV can be obtained by studying polarized observables which are often more sensitive to the details of the mechanism than cross sections. In particular, it is important to study the asymmetry of the reaction (1) cross section:

$$\Sigma = \frac{d\sigma_\parallel - d\sigma_\perp}{d\sigma_\parallel + d\sigma_\perp} \tag{2}$$

where $d\sigma_{\parallel(\perp)} = d\sigma_{\parallel(\perp)}/d\Omega$ is the cross section in the case when the photon polarization vector is parallel (perpendicular) to the reaction plane. First, according to [9], the model of ref. [3 - 6] and the meson theory give qualitatively different predictions. Second,

the asymmetry for photon energies from 1 $\rightarrow$ 2 GeV is very sensitive to the presence of nucleon configurations in the deuteron wave functions.

This experiment is relatively simple. It does not require:

-high electron currents;

-complicated detector systems for reaction product detection;

-performing absolute measurements.

Hence, the experiment can be run at the first stage of the development of experimental methods and the use of the CEBAF accelerator.

Physics Motivation

Constituent counting rules

At the present time quantum chromodynamics describes well enough a number of hard processes. For instance, constituent counting rules [3 - 6] predict, at high energies, a definite behavior of hadron form factors and the cross sections of exclusive reactions. In particular, the dependence of the differential cross sections on the total energy squared s at a fixed value of the angle θ_p^{cm} in the center-of-mass system is predicted to have the form:

$$\frac{d\sigma}{dt} \approx s^{n-2} \tag{3}$$

where n is the total number of quarks, photons, and other fundamental particles in the initial plus final states in the reaction. This prediction of the quark models has been confirmed by experiments on NN scattering and pion photoproduction, $\gamma N \rightarrow \pi N$. The scaling dependence of $pp \rightarrow pp$ and $\gamma N \rightarrow \pi N$ cross sections has been observed at high energies of incident particles ($s/m^2 \geq 15$ and 7 for the first and the second reactions, respectively, where m is the nucleon mass), and in the case of $pp \rightarrow pp$ scattering the phenomenon has been observed in a wide range of angles (Fig. 1). The dependence of π, p and n form factors on Q^2 also agrees with the theory quite well. Concerning the reaction (1), a hint of scaling behavior of the cross section was obtained in the first SLAC experiment [1] at comparatively low energies $E_\gamma \approx 1.4$ GeV ($s/M_d^2 \approx 2$, where M_d is deuteron mass). The data of ref. [1] and preliminary results of the second SLAC experiment [2] show that for $\theta_p^{cm} = 53^o$ and 90^o the cross section energy dependence is described by Eq. (3) ($n = 12.1 \pm 0.8$ for $\theta_p^{cm} = 90^o$ and $n = 11.0 \pm 0.5$ for $\theta_p^{cm} = 53^o$) starting with $E_\gamma \approx 1 \rightarrow 1.2$ GeV (Fig. 2).

However, the data for $\theta_p^{cm} = 37^o$ essentially differ from the predictions of the constituent counting rules. The dependence observed is also of the form (3), but $n = 8.7 \pm 0.3$ (Fig. 2c). This result points either to the variation, with the proton production angle, of the number of interacting elementary fields in the reaction (1), or, more probably, points out that at the present time it is not clear what factors (quarks or nucleons) cause the behavior of the process (1) cross section in the energy range of 1 $\rightarrow$ 2 GeV. Thus, the prediction of asymptotic scaling in the reaction (1) requires experimental confirmation.

Meson theory

In ref. [2], the experimental data of ref. [1, 2] were analyzed and compared with the results of calculation of ref. [10, 11], which had been performed within the framework of the conventional meson theory. It was shown that the results of [10] do not agree with the experimental data for practically all angles at $E_\gamma \geq 1$ GeV (Fig. 3). The most considerable disagreement was for $\theta_p^{cm} \leq 53^o$.

The calculations of ref. [11] used a Hulthen wave function, and took into account the excitation of virtual resonances with $J \leq 5/2$ and the exchange of π, ρ and η mesons. The results show good agreement with the SLAC experimental data for $\theta_p^{cm} = 90^o$ and for energies up to 1.5 GeV. However, as was noted in ref. [2], this good agreement is apparently achieved owing to the use of an energy dependent cutoff.

In ref. [9] a detailed study of the reaction (1) at $E_\gamma > 1$ GeV was carried out in a Lorentz-covariant approach. The deuteron wave function used for the computation contained nucleon $|NN>$ and Roper configurations. ($N(\frac{1}{2}^+, 940)$ stands for the nucleon and $N^*(\frac{1}{2}^+,1440)$ stands for the Roper resonance.) The model of ref. [12] was used as the dynamical model of dNN and dNN^* vertices. It was assumed that for dNN and dNN^* the rates of the form factor decrease are equal and described by the following expression:

$$G\left(-k^2\right)_{N(N^*)} = C_{N(N^*)}[\beta^2_{N(N^*)}/2 + \alpha_0^2 - k^2]^{-\epsilon} \tag{4}$$

The rate of form factor decrease is described by one parameter $\epsilon = 3; \epsilon = 4$ corresponds to the asymptotic condition. The values of other parameters, which are the same for the NN and NN^* configurations, are: $\alpha_0^2 = 0.002m^2$, where m is the nucleon mass, and $\beta^2 = 0.02m^2$. The ratio of the dNN to the dNN^* vertex form factor (in the asymptotic region of the theory) is determined by a single parameter $\alpha = C_{N^*}/C_N$. The value of C_N was fixed by matching the theoretically calculated cross section to the experimental data [1] at $E_\gamma = 1$ GeV and $\theta_p^{cm} = 90^o$.

The results of theoretical calculations [9] of the differential cross section are shown in Fig. 4a. Continuous curves 1 and 2 correspond to the calculations without taking into account the NN^* configurations ($\alpha = 0$). Curve 2, corresponding to the asymptotic case ($\epsilon = 4$), is in good agreement with the results of ref. [13] (crosses), which assume scaling behavior for the process amplitudes. The dashed curve was obtained by taking into account the NN^* configurations with $\alpha = 15$ and $\epsilon = 3$. One can see that for $\theta_p^{cm} = 90^o$, the SLAC experimental data [1,2] are in rather good agreement with the predictions of meson theory [9] up to the photon energies of $E_\gamma \approx 2.2 \rightarrow 2.4$ GeV, when the NN^* configurations are taken into account in the dNN and dNN^* vertex models [12]. At higher energies, considerable disagreement of the theoretical calculations at $\epsilon = 3$ with the experiment is seen. Better agreement is obtained when the asymptotic behavior ($\epsilon = 4$) of the dNN vertex form factor is assumed. According to [9] in the region $E_\gamma \geq 2.4$ GeV the behavior of the amplitudes seems to change, and the scaling predicted in [3 - 6] can exist at energies above 2.4 GeV.

One of the important conclusions of [9] is that in the framework of meson-nucleon theory one can get, for large ϵ, a factorized form of the reaction (1):

$$\frac{d\sigma}{d\Omega} \approx Const * f\left(\theta, s\right)/s\left(s-1\right)^{2\epsilon-1} \tag{5}$$

which, for $\theta_p^{cm} = 90^o$, f(90°,s) = 1, and $\varepsilon = 3$ in the energy range $E_\gamma = 1 \rightarrow 3$ GeV ($s = 8 \rightarrow 16$ GeV), can imitate the energy dependence of the cross section in the form:

$$\frac{d\sigma}{dt} \approx s^{-11 \text{or} -12}, \tag{6}$$

which coincides with that predicted by the constituent counting model [3 - 6]. Hence, within the 1 - 3 GeV region the cross section energy dependence (6) itself can not be

considered as the serious argument for the QCD mechanisms of real photon absorption in this energy range. To solve the problem data on other observables are required.

Another important conclusion of [9] is that f(θ, s), (where only the NN configuration is taken into account) is almost independent of s only in the angle interval:

$$50^o \leq \theta_p^{cm} \leq 130^o. \tag{7}$$

Thus, the energy dependence (6) can take place only within this angle interval. Beyond the interval (7) the rate of cross section falloff with varying s decreases, and $s^{11}\ d\sigma/dt$ becomes an increasing function with the rate of increase being higher in the region of forward scattering angles than in the region of backward scattering angles. The SLAC experimental data [1, 2] qualitatively confirm this conclusion (Fig. 4b).

Apparently, the model [9] provides a correct general picture of the process, at least for energies up to 2.4 $\rightarrow$ 3.0 GeV. If it is true, the photon interacts with nucleons and not with quark configurations, and scaling is not observed for this energy region.

Fig. 5a presents the results of calculations of the cross section (2) asymmetry for $\theta_p^{cm} = 90^o$. The dotted curve corresponds to the case when only the NN configurations are taken into account in the deuteron wave function. Curves 1, 2, 3, and 4 for α = 10, 15, 20, and 30, respectively, correspond to the case when the NN^* are taken into account. One can see that the asymmetry is very sensitive to the presence in the deuteron ground state of the addition of resonance configurations. The inclusion of the latter results in a factor of several decrease in the asymmetry magnitude. Theory predicts the most abrupt change in the asymmetry behavior for $\theta_p^{cm} \leq 60^o$, where the asymmetry magnitude decreases from 0.7 to $\approx$ 0. (Fig. 5b). This effect is a general consequence of the presence in the deuteron of the non-nucleon configurations.

In contrast to the cross section the asymmetry is weakly dependent on the rate of the form factor falloff in the dNN vertex.

The theoretical calculations of the asymmetry are in good agreement with experimental data [14] obtained at $E_\gamma \leq 1$ GeV.

It is very important that the predictions of the model [9] and of the constituent counting model [3 - 6] for the asymmetry at $\theta_p^{cm} = 90^o$ and in the energy range 1 $\rightarrow$ 3 GeV are essentially different. The expected value of the Σ asymmetry in the asymptotic scaling mode is:

$$\Sigma \approx -1 \tag{8}$$

independent of the deuteron structure, while the model [9] predicts, under the same conditions, the asymmetry value to be close to zero. Thus, the measurement of the asymmetry may become a strong criterion for the presence or absence of the asymptotic scaling. It will allow one to answer the question of whether or not quark states of freedom manifest themselves in deuteron photodisintegration in the given energy region.

According to [9] the theoretical parameter α can be expressed through such physical parameters as the mean square radii r_N and r_{N^*} of the NN and NN^* configurations and the admixture of the NN^* component in the deuteron:

$$\alpha \approx \left(\frac{\xi}{1-\xi}\right)^{1/2}\left(\frac{r_N}{r_{N^*}}\right)^{5/2}\left(\frac{m}{M_{N^*}}\right)^{1/2}\left(\frac{m+M_{N^*}}{2m}\right) \tag{9}$$

where ξ is the admixture of the NN^* configuration in the deuteron wave function, and m and M_{N^*} are the nuclear mass and the nucleon resonance mass, respectively. The

comparison of the calculations with experimental data [14] restricts α values to be from 10 to 15. In [9], with taking $r_N \approx 2$ fm and assuming that NN^* admixture is about 2%, it was found that the NN^* configuration radius is within the following interval:

$$0.33 \leq r_{N^*} \leq 0.38 fm \tag{10}$$

This is in good agreement with the nuclear core radius in NN potentials.

The estimates of the role of the off-shell effects carried out in [9] shown that these effects are not able to shadow the non-nucleon component effects in the deuteron wave function (Fig. 4 and 5).

Thus, the asymmetry measurement in a region of $1 \rightarrow 2$ GeV will allow one to check the theoretical predictions [9] of meson theory and, if the latter gives the correct description of the process (1), to study the non-nucleonic configurations in the deuteron wave function.

General description of proposed experiment

We propose to measure the energy dependence of the cross section asymmetry of $\gamma d \rightarrow pn$ in the photon energy range $E_\gamma = 0.6 \rightarrow 2.4$ GeV at $\theta_p^{cm} = 30^o$, 90^o and 150^o, and to measure angular distributions for $E_\gamma = 1.0$, 1.4 and 2.0 GeV.

The experiment will be carried out with a linearly polarized photon beam obtained by the interaction of electrons with a diamond single crystal. The separation of the reaction under investigation from competing processes will be performed with the help of pn coincidence measurements.

Because of a considerable decrease in the reaction cross section with increasing energy, running the experiment requires high luminosity and equipment which is capable of operating under the conditions of high counting rates. Hence, in the nearest time the measurements at energies above 1.5 GeV can be performed only at CEBAF in Hall A or C. Since in these halls there is no equipment for the generation of pure photon beams we propose to run the experiment with either mixed $\gamma + e^-$ beam, or to develop a compact magnetic system for spatial separation of the γ and e^- beam and to run the experiment with the pure photon beam. Both variants are described below.

One of the conditions substantially simplifying the problem is that the proposed experiment does not need electron beam currents above 30 μA.

Variant A. Experiment with mixed $\gamma + e^-$ beam

The experimental set up is shown in Fig. 6. The electron beam strikes a diamond single crystal target for producing photons. The target is suitably fixed in a goniometer. Two places for placing the goniometer are possible:

-before the second raster magnet at a distance of $\approx$ 3 m from the deuteron target (position 3A, Fig. 6);

-behind the second raster magnet at a distance of $\approx 0.7 \rightarrow 1$ m from the deuteron target (position 3B, Fig. 6).

Since in the present experimental scheme the deuteron target is irradiated by photons and electrons, it is necessary for subtracting the electrodisintegration contributions to perform measurements with the photon target removed. This circumstance results in a several times increase in the time required for the experimental run.

i) Single crystal target. Spectra and polarization.

The calculations of expected yields of *pn* coincidences in the photo- and electrodisintegration processes show that the photon target width should be not less than $0.05 \rightarrow 0.06$ X_0 for the electrodisintegration contributions to be not more than 50%. If as the photon target one uses a diamond crystal ($X_0 = 12.8$ cm), as is most often used for getting polarized photon beams due to its high Debye temperature, the diamond thickness should be ≈ 6 mm.

Fig. 7 shows the photon spectra and polarization expected in the case where the 6 mm thick single crystal target is oriented relative to the electron beam in such a way that the main contribution to the coherent bremsstrahlung cross section is made by a single reciprocal lattice point $(2, \bar{2}, 0)$. Initial electron energy is $E_0 = 4$ GeV. $(2, \bar{2}, 0)$ orientation is most often used in the experiments, since it allows one to obtain higher polarization than one obtains in the other possible orientations. The expected polarization varies from ≈ 0.6 at $E_\gamma = 1$ GeV to ≈ 0.25 at $E_\gamma = 2.4$ GeV. To prevent a considerable decrease in the coherent effect, which reduces the radiation polarization, the angular divergence of the electron beam should be several times less than the multiple scattering angle,

$$\theta \leq \theta_{sc}$$

For the 6 mm thick crystal the limit on angular divergence is $0.1 \rightarrow 0.15$ mrad.

ii) Single crystal orientation

Crystal orientation is a procedure which consists in aligning one of the main crystal axes, for example $\vec{B}_1 =< 110 >$, with the beam axis $\vec{P}_0$, and the two other axes, $\vec{B}_2 =< 1\bar{1}0 >$ and $\vec{B}_3 =< 001 >$, with the horizontal and vertical rotation axes of the goniometer. When performing the procedure one usually makes special measurements of the orientation dependence of photon beam intensity with an ionization chamber or a quantometer. Since in Hall A and Hall C there are no magnets to clean the photon beam from the charged component, it is not possible to directly use this conventional method.

An experimental test of methods for single crystal orientation which can be used in CEBAF Hall A, when working with the mixed $\gamma + e^-$ beam, was carried out with the Kharkov LINAC at an electron energy $E_0 = 1.2$ GeV, and with a diamond crystal thickness of 1.8 mm. Studied have been three possible orientation methods which are based on the orientation dependence of the following effects:

-secondary electron emission from the crystal;

-the passing of the scattered electron beam through a collimator;

-gamma radiation of electrons in the crystal.

To our point of view the third method seams to be the most promising for the Hall A conditions. The method is a modification of a conventional method consisting in measuring the orientation dependence of the intensity of the gamma radiation of electrons in the crystal. To apply this method in Hall A it is necessary to bend the electron beam that passed through the crystal by a small bending magnet in such away that before getting a beam dump the beam would pass aside from the ionization chamber. To this end the bending magnet is installed straight behind the deuteron target (Fig. 6); the ionization chamber is located at a distance of ≈ 20 meters from the deuteron target. In this case the deviation of the electron beam by an angle of ≈ 3 mrad will cause a shift of the beam

at the vicinity of the ionization chamber by a distance of ≈ 60 mm. When the electron beam passed through the diamond crystal (6 mm thick) and the deuteron target (10 cm thick) the multiple scattering angle is ≈ 1 mrad at the initial electron energy of 4 GeV. Beam dimensions caused by the multiple scattering will be $\approx \pm 20$ mm at the vicinity of the ionization chamber.

A magnet with a field strength of ≈ 3 kilogauss and a magnetic pathway length of $\approx 12 \rightarrow 13$ cm is enough for deviating the electron beam with $E_o = 4$ GeV by 3 mrad. A similar second magnet is used for turning the beam and directing it into the beam dump.

Crystal orientation will be carried out at lower electron beam intensity ($\approx 0.01 \rightarrow 0.001\ \mu A$); hence, problems of radiation security are reduced. Upon finishing the crystal orientation, the magnets are turned off.

The orientation dependence of the photon beam intensity obtained by the procedure described above with the Kharkov linear accelerator (the deviated electron beam passed at a distance of ≈ 20 cm from the ionization chamber) were practically the same as obtained with the conventional measurement scheme.

iii) Determining the polarization

We propose to determine the degree of photon polarization in the region of the maximum of the coherent peak by measuring the orientation dependence of the reaction (1) yields $C_{\|(\perp)}(\theta_p, P_p; \theta_{cr}, \alpha)$ (for photons polarized parallel and perpendicular to the reaction plane) at fixed values of the kinematic parameters θ_p and P_p (the angle and the momentum of the outgoing proton) corresponding to the chosen value of photon energy. θ_{cr} and α are crystal orientation angles (θ_{cr} is the angle between the electron momentum $\vec{P}_o$ and $\vec{B}_1$ axis and α is the angle between plains ($\vec{P}_o$, $\vec{B}_1$) and ($\vec{B}_1$, $\vec{B}_2$). These angles unambiguously determine the location of the interference peak E_γ^p in the spectrum of coherent bremsstrahlung. In the case when the main contribution into the coherent bremsstrahlung cross section is made by the single reciprocal lattice point $(2, \bar{2}, 0)$ the effective polarization near the peak is [15]:

$$P_\gamma = k\Big[\frac{2(1-x)}{1+(1-x)^2}\Big]\frac{\beta-1}{\beta} \tag{11}$$

where $x = E_\gamma/E_o$, $\beta = (C_\|^{max} + C_\perp^{max})/2C_a$, $C_{\|(\perp)}^{max}$ is the proton yield in the maximum of the orientation dependence $C_{\|(\perp)}$ for the two directions of the polarization vector, and C_α is the yield under the same kinematic conditions, but measured with the disoriented crystal. A coefficient k takes into account a small contribution into the coherent bremsstrahlung cross section from the reciprocal lattice points of the diamond crystal next to $(2, \bar{2}, 0)$; k varies from 0.98 to 0.9 with x varying from 0.1 to 0.4. The advantage of the method for determining the polarization is connected with the fact that the presence in the reaction yields $C_\|$, $C_\perp$ of noncoherent background (from the background reactions with $P_\gamma \Sigma \approx 0$) does not affect the value of asymmetry due to the taking into account of the background in the value of effective polarization.

iv) Radiation damage and heating of the crystal

To diminish radiation damage on the crystal it is proposed to use in the experiment electron beams of $1 \rightarrow 2$ mm in diameter. Electron beams of these dimensions are used in experimental studies with the Kharkov linear electron accelerator for obtaining polarized photon beams on diamond crystals with a thickness up to 2 mm ($\leq 0.015 x_o$). The

expertise acquired showed that the single crystal conserves its properties, until getting an integral dose of $\approx 10^{21}\ e^-/cm^2$, during long cycles of work with pulsed electron beams at average current up to 2.5 μA (pulsed currents of $\approx 50\mu A$) without applying any special means for heat removal. Upon getting this dose, the mechanical destruction of the crystal is possible. This dose will be acquired during $\approx$ 50 hours of continuous running of the CEBAF accelerator at a current of $30\mu A$ and a beam diameter of 2 mm, or during 150 hours at a current of $10\mu A$. Shifting, during the measurement, the beam entering the crystal by $1 \rightarrow 2$ mm with the help of the raster magnet will increase the lifetime by $3 \rightarrow 4$ times. According to the estimates of required statistics (Table 4) and measurement time (Table 5) the experiment can be performed with one or two crystals.

Difficulties connected with the use of high electron currents are mainly caused by the local overheating of the crystal, which can lead to the destruction of the lattice. However, these difficulties cause serious troubles only for the measurements in the energy region above 1.6 GeV, when one needs to use high electron currents of $\approx 30\mu A$. The magnitude of power lost in the crystal at a current of 30 μA is

$$P = (dE/dx) * I * L \approx 120\text{W}$$

for the crystal with $L = 6$ mm ($dE/dx = 6.7$ MeV/cm for the diamond) and $P \approx 10$ W for the crystal with $L = 0.5$ mm. The specific power loss in case of the beam being 2 mm in diameter is ≈ 3.9 and 0.65 kW/cm^2, respectively.

Calculation of crystal heating shows that, under the conditions of heat equilibrium, temperature in the region of the beam (in the center of the crystal) will be by $\approx 20°$ higher than at the crystal boundary, provided $I_e = 30$ μA, beam diameter is 0.2 cm, crystal diameter is 1 cm and the temperature of a side wall of the crystal is kept at 20° C = 293 K. This should not be difficult. Similar values (≈ 0.5 kW/cm^2) of specific power loss were obtained in an experiment [17] with the Darmstadt linear accelerator at an electron energy of ≈ 5 MeV.

The crystal is able to withstand high pulsed current load. For example, on the Kharkov LINAC during the current cycle ($\approx 1\mu$s) an energy of approximately 55 kDj ($\approx$800 kDj/cm^2) is released in a crystal of thickness 0.2 cm, and is dissipated naturally without actively cooling the crystal during the time between the current cycles (0.02 sec). With the aim of decreasing the deposition of the heat energy in the crystal we are planning limit the beam current to values of $\approx 5\mu$A for the 6 mm thick crystal and $\approx 30\mu$A for the 1 mm thick crystal. This corresponds to a power loss in the crystals ≈ 20 W.

v) Deuteron target

We propose to use in the experiment the liquid deuterium 10 cm-long target being developed by California State University at Los Angeles and CEBAF [16]. This target is designed for electron beams as small as 0.1 mm in diameter, currents up to 200μA, and a power loss in the target up to 1 kW. The requirements to the target in this experiment are not so high – the currents are to be not more than 30μA and electron beam dimensions are to be ≈ 2 mm. If required, scanning of the electron beam on the target will be carried out when performing measurements in the energy range above 1.6 GeV.

vi) Reaction identification

In contrast to the SLAC experiments [1, 2], where the measurements were performed at the end of the bremsstrahlung spectrum, the reaction (1) yield in the experiment proposed

herein should be measured in the photon region near the maximum of the coherent peak, which should be located within the relative energy range $x \leq 0.5$ for the degree of photon polarization to be high enough. Thus the conditions of the reaction identification will be essentially different. To single out the reaction (1) from the background of the competing contributions it is necessary to measure *pn* coincidences.

For detecting protons we propose to use the hadron spectrometer (HRS) of Hall A with its standard detectors.

To detect neutrons, it might be possible to use one of the three neutron detectors currently planned for Hall A. The neutron polarimeter of Dick Madey of Kent State for the neutron electric form factor experiment (89-005) could be used instead simply as a neutron detector. The high resolution detector planned by John Watson of Kent State would be very appropriate, especially for the higher neutron energies at which sufficient energy resolution must be maintained to eliminate events in which π production occurred. Finally the HARP collaboration plans to bring their neutron detector, which is currently under construction, to CEBAF after finishing a series of experiments at NIKHEF. We have started discussions with these groups concerning the use of their detectors for this experiment. These discussions should be complete by the time of the PAC. For now, we will assume that a new detector is needed, and describe it below.

To detect neutrons, we propose to use a hodoscope of 12 scintillation counters 20 cm thick, 10 cm wide and 16.2 cm high (hodoscope total dimensions are 30 cm in horizontal and 65 cm in vertical direction). The hodoscope is to be placed 5 m from the deuteron target center when the measurements are performed at an angle of 90^0. These geometrical dimensions allow one to match the solid angles of the proton and neutron arm when detecting pn coincidences. To suppress charged particle background, scintillator counters for anticoincidence vetoes are placed in front of each neutron counter.

The neutron counter is shielded by concrete blocks. A lead absorber 10 cm thick (17.68 X_0) is proposed to be placed in front of the counter for decreasing the loading of the counters with charged particles and photons. With the purpose of more reliable separation of deuteron photodisintegration we propose, besides the angle, to measure neutron energy by using time of flight.

vii) Estimates of count rate in proton and neutron channel

Estimates of the expected count rates in the proton and neutron arms under the kinematic conditions of the experiment (Table 1) are presented in Table 2. In the calculations it was assumed that:

- the solid angle of the spectrometer is 7 msr, momentum acceptance is $\pm 5\%$ and proton detection efficiency is 100%;
- the low-temperature liquid deuterium target is 10 cm long ($0.51 * 10^{24}$ nuclei/cm^2);
- the fraction of neutrons passing through the 10 cm thick lead absorber is 0.57, neutron detection efficiency is 0.2;
- the thickness of the input and output aluminum window of the deuteron target is 0.1 mm;
- the photon target is a diamond single crystal of thickness 6 mm;
- electron beam energy is $E_0 = 4$ GeV;
- the solid angle of the neutron counter is matched to the angular acceptance of the spectrometer.

To calculate the $d(\gamma,p)n$ reaction yield the number of real photons for the oriented

and disoriented diamond crystal were estimated in the energy range specified by reaction kinematics and ±5% momentum acceptance.

The data on differential cross sections of the $d(\gamma,p)n$ reaction was taken from the SLAC experiments [1,2], and extrapolated to the regions where the data are absent (Table 1).

The differential cross sections of the background reactions due to photon and electron interactions with the deuteron target and target walls were calculated in the standard way [18]. The number of equivalent photons was calculated for the disoriented diamond target (similar to an amorphous target of the same thickness).

Table 2 presents the results of the calculations of the yields of deuteron photodisintegration from the interaction of bremsstrahlung and coherent radiation with the deuteron target, and also the proton and pion yield in the photo- and electrodisintegration of the deuteron. The expected total counting rate caused by protons and all other charged particles is presented. Since the contribution of the target walls into the total particle yield was not higher than $5 \rightarrow 10\%$, the calculation of the former are presented only for an angle of 90^0.

Additional count rate in the proton arm, caused by photo- and electrodisintegration in the diamond radiator target will be practically absent, because the spectrometer does not "see" the photon target. Additional line of sight neutron shielding may be required for the spectrometer detectors. Count rate in the neutron arm will increase approximately two times. However, to decrease the count rate we propose to use a concrete shielding wall ≈ 1 m thick, which is placed near the goniometer. The wall will allow one to almost completely get rid of the background from the photon target in the neutron detector.

The calculations show that the neutron arm count rate does not exceed 10^5 sec^{-1}. Under these conditions the detection system will be able, with high efficiency, to suppress the background of pions, positrons and other charged particles. The expected count rate of protons for these angles does not exceed $1 \rightarrow 2 \times 10^4$ s^{-1}. At $\theta_p^{cm} \geq 90^0$ the contribution of electrodisintegration is predominant.

The count rate of the counters of the neutron telescope includes the neutrons as well as the charged particles. To estimate the counting rate, the calculated spectral distributions of protons, pions and neutrons were integrated over particle momentum in the range from 50 to 1700 MeV/c, taking into account particle absorption in the lead absorber and neutron detection efficiency. In Table 3 the results of count rate calculations are shown for charged particles (pions) and neutrons appearing as a result of photo- and electrodisintegration. The target wall contribution is small and was not taken into account. The charged pions are the main contribution into the count rate of the neutron counter. The neutron count rate is lower by an order of magnitude. As in the case of the proton arm the main contribution into the total count rate is made by the electron component of the mixed beam. Since the total count rate of each neutron counter of the hodoscope does not exceed 10^5 s^{-1} suitable electronics with a time resolution of $10^{-8} \rightarrow 10^{-9}$ sec will ensure efficient suppression of the charged particle background.

viii) Count rate of proton neutron coincidences

The count rate of pn coincidences was calculated with an assumption of a match of the solid angles of the proton and neutron arm. The absorption of neutrons by the lead absorber and neutron detection efficiency were taken into account in the calculations. The yield for the oriented ($d(\gamma,p)n$ cryst.) and disoriented ($d(\gamma,p)n$ amorph.) crystal as well as the yields caused by the virtual photons $d(e,p)n$ were calculated. The results

are presented in Table 4. One can see that for the oriented crystal the ratio of the $d(\gamma,p)n$ yield to the $d(e,p)n$ yield is substantially higher than for the disoriented crystal. The magnitude of the accidental coincidences was estimated from the total count rate in the proton (total p, amorph.) and neutron (total n) arm with resolution time of the coincidence assumed to be $\approx 2 * 10^{-9}$ sec.

ix) Required statistics and beam time for the experiment

If one neglects the contribution of background pn coincidences from the target walls, the experiment proposed herein implies that the measurements of the yield of pn coincidences should be performed under the following conditions:

- with the mixed $\gamma + e^-$ beam (when the polarization vector is parallel ($C_{\|}$) or perpendicular ($C_{\perp}$) to the reaction plane, or the crystal is disoriented (C_a);
- with the pure electron beam C_e (without photon target).

The asymmetry is determined by the following expression:

$$\Sigma = \frac{1}{P_\gamma} \frac{C_{\|} - C_{\perp}}{C_{\|} + C_{\perp} - 2C_e} \tag{12}$$

The polarization magnitude P_γ is calculated in accordance with (11) by using data on $C_{\|} - C_e$, $C_{\perp} - C_e$ and $C_a - C_e$ yields which have been measured.

The statistics for $C_{\|} + C_{\perp}$, C_a and C_e for ensuring the required precision for the asymmetry $\Delta\Sigma$ measurement are shown in Table 5. Time requirements were estimated with the use of values of $C_{\|} + C_{\perp}$, C_a and C_e and the corresponding count rates of pn coincidences (which are presented in Table 4). The estimates were performed with the use of the calculated values of photon beam polarization; the asymmetry value for $E_\gamma \leq 1$ GeV and $\theta_p^{cm} = 90^0$ were taken from [14], while for other experimental conditions they were considered to be at a level of $\Sigma = 0.15$. It should be noted that the required statistics are weakly dependent on the asymmetry magnitude.

Time for gaining the required statistics is estimated to be 160 hours. Time for measurements at angles of 60^0 and 120^0 for getting angular distributions at 1.0, 1.4 and 2 GeV is $\approx$ 50 hours. The total time for gaining statistics is $\approx$ 210 hours. The total time for running the experiment is presented in Table 9.

Variant B. Experiment with the separation of γ and e^- beam

Experimental set up

The experimental set up for Variant B is shown in Fig. 9. The goniometer setup is placed at a distance of 3 $\rightarrow$ 3.5 m from the deuteron target before the second raster magnet. Immediately behind the goniometer a magnetic system with two dipole magnets is located. The system shifts the electrons, which have passed through the crystal, in the transverse direction. It is designed in such a way that the electrons with maximum energy are shifted by 10 $\rightarrow$ 12 mm and guided, in parallel to the incoming beam axis, beside the deuteron target into the beam dump.

After passing through the crystal the electron beam has an energy spectrum from 0 to E_o; it is not monochromatic. However, in contrast to the photon component, the spectrum of energy of the scattered electrons has a maximum near the maximum energy E_o (Fig. 9). The calculation performed for a crystal of thickness 0.5 mm, a beam current of $30\mu A$ and an initial energy of $E_o = 4$ GeV shows that $\approx$ 97% of the energy of the beam scattered electrons is contained in the spectrum range from 2 to 3.975 GeV and 98.3% of

the energy is in the interval from 1.5 to 3.935 GeV (the total power of the scattered beam is $\approx$ 2000 W). Thus, when the energy acceptance of the system is $(0.5 \rightarrow 1) \times E_o$, the scattered power not accepted by the system is $\approx$ 3% (i.e. $\approx$ 60 W), and it is 1.7% ($\approx$ 30 W) at an acceptance of $(0.375 \rightarrow 1) \times E_o$.

Fig. 10 demonstrates the geometry and the dimensions of the electron and photon beam for one of the types of the symmetric magnetic system designed with the "Transport" program. The system consists of two identical dipole magnets with cut angles of the incoming and outgoing bound of $\approx 33^\circ$ and a gap of 10 mm. The magnetic field is 10 kG, the length of the magnetic pathway for the beam particles with an energy of 4 GeV is 25.8 cm and the distance between the magnets is 25.8 cm. The energy acceptance of the system is from 1.5 to 4 GeV. The system shifts the main particle by 10 mm and has the focal point at a distance of $\approx$ 15 m from the outgoing cut of the second magnet. In the calculations, the electron beam entering the magnetic system (after the crystal) was assumed to have a dimension of $\pm$1 mm and an angular divergence of 0.16 mrad caused mainly by multiple scattering in 0.5 mm thick diamond. The divergence of the electron beam striking the crystal was assumed to be 0.1 mrad.

Thus, upon passing through the magnetic system the photon and electron beam are separated and move in the same vacuum pipe at a small distance from each other. Only the photon beam strikes the deuteron target. At the vicinity of the target the vertical dimensions of the beams do not exceed $3 \rightarrow 4$ mm, the maximum horizontal dimension at the exit of the magnetic system does not exceed 21-22 mm.

Experimental techniques and procedures

In the present variant of the experiment the deuteron target is irradiated only by photons. Hence, the experimental procedure is similar to, but becomes essentially simpler, than the technique described above. The count rates and, as a consequence, the requirements for the detectors, become substantially lower.

i) Single crystal target

The orientation of the single crystal photon target relative to the electron beam is the same as in the first variant. The methods for crystal orientation and polarization measurements also remain the same. Since the electron and photon beams have been spaced apart, performing crystal orientation does not require the installation of the bending magnet after the scattering chamber.

The optimum thickness of the crystal in the variant under consideration is $0.5 \rightarrow 1$ mm. In this case the polarization and the coherent effect will be substantially higher than for the 6 mm-thick crystal, especially at energies $\leq 1.2 \rightarrow 1.4$ GeV (Fig. 7c, d); hence, the required statistics can be lower.

The power loss for the thickness given above does not exceed 20 W at a current of 30μA.

ii) Reaction identification and count rate estimate

The identification of the reaction is carried out by detecting pn coincidences. However, in this case the counting rate of the counters is $5 \rightarrow 10$ times smaller. The estimates for count rate magnitudes under conditions of Variant B are shown in Tables 6 and 7. Even for small angles $\theta_p^{cm} < 60^\circ$ the count rate does not exceed 10^4 s^{-1} (at a current of 1μA). The level of accidental coincidences becomes substantially lower as well.

iii) The count rate of pn coincidence and beam time for running the experiment

The count rate of pn coincidences is caused only by photons.

To determine the asymmetry in the case under question one should measure the yields $C_{\|}$, $C_{\perp}$ and C_a of pn coincidences. If the target wall contribution is neglected, the asymmetry magnitude is determined by the expression (12) where $C_e = 0$.

Statistics required for $C_{\|} + C_{\perp}$ and C_a, which ensure the accuracy of the asymmetry $\Delta\Sigma$, are presented in Table 8. It is essentially lower than that in Variant A because of the absence, in Variant B, of the electrodisintegration background. There is a possibility of extending the photon energy range of measurements up to 2.4 GeV. The estimates of the pure time for the experiment with the 0.5 mm - thick crystal are presented in Table 8 and are $\approx$ 160 hours. From our point of view, the present variant of the experiment is preferable.

Total time requirements

Running the experiment also requires additional beam time:

-50 hours for the calibration of equipment and test measurement;

-60 hours for performing crystal orientation, and changing the energy of the interference maximum (coherent peak energy), angles and spectrometer magnetic field;

-50 hours for measurements with the empty target.

The total time for Variants A and B of the experiment with crystals of different thickness is shown in Table 9. This time is 365 hours for Variant A and 390 hours for Variant B (0.5 mm - thick crystal). For Variant B the energy range accessible for measurements is larger than that for Variant A by 200 MeV.

At the first stage of the experiment one may restrict oneself by measuring only two energy dependences of the asymmetry (for angles of 30° and 90°) and three angular distributions. In this case the total time for the experiment is $\approx$ 250 hours for Variant A, and $\approx$ 280 hours or 200 hours for Variant B with the crystal of thickness 0.5 mm and 1 mm, respectively.

If the investigations of diamond crystal heat resistance, which we are planning to carry out, show that the electron current can be increased, for instance, two times, it will be possible to further decrease the time for the measurements by $\approx$ 30% in comparison with the values presented above.

The experiment results expected for Variant A are presented in Fig. 4.

Tests and reliability of the experimental procedure

A one arm simulation test of the experimental procedure for measuring asymmetry with the mixed $\gamma + e^-$ beam has been carried out with the Kharkov accelerator. The experimental setup was the same as that shown in Fig. 6. A diamond crystal of thickness 1.8 mm used for the measurements was oriented in the experimental hall with the mixed $\gamma + e^-$ beam by the method which we propose to use for the experiment in CEBAF Hall A (see above). The experimental conditions were the following:

-electron energy was 1.7 GeV;

-coherent peak energy was 300 MeV;

-a cryogenic target had two sections each of diameter 40 mm and length 200 mm. One of these was filled with liquid deuterium and the other was filled with liquid hydrogen;

-proton detection angle was $\theta_p^{cm} = 90°$. The protons were detected by a magnetic spectrometer and a telescope of scintillator counters.

The orientation dependence of the yields of the deuteron photodisintegration with subtracted electrodisintegration background is shown in Fig. 11 for two cases, when the polarization vector of the photon beam is parallel and perpendicular to the reaction plane. The electrodisintegration background was $\approx 80 \rightarrow 85\%$, which practically agrees with the calculations. The effective polarization calculated in accordance with Eq.(11) was $\approx$ 63%. The asymmetry magnitude obtained is in agreement with earlier experimental data obtained in [15] (Fig. 4c), which testifies to the capabilities of the proposed experimental technique. The accuracy of the proposed procedure for the asymmetry measurement is confirmed by the results of recent measurements of the asymmetry of the $\gamma d \rightarrow pn$ and $\gamma p \rightarrow p\pi^o$ reaction performed in Brookhaven [19] with a linear polarized photon beam produced as a result of the Compton scattering of laser radiation on relativistic electrons (Fig. 12). The data obtained in these experiments are in good agreement with the data [15, 20, 21] obtained with the proposed procedure in Kharkov.

Collaboration

The experiment proposed may be considered as part of the experimental program for studying the deuteron photodisintegration process in Hall A. The main part of the experiment may be carried out simultaneously with measurements of proton polarization in the same reaction [8].

KhPTI can take upon itself work on obtaining the polarized photon beam, developing the magnetic system for the separation of the electron and photon beam in Hall A (Variant B of the experiment), producing single crystal targets and their preliminary orientation with the KhPTI linear accelerator and studying the radiation resistance of the crystals at high electron currents. KhPTI can also take upon itself work on the construction of the neutron detector, if required. The KhPTI also intends to test the proposed measurement procedure with the mixed beam under realistic conditions for energies up to 0.8 GeV.

It should also be noted that if Variant B of the experiment (with separated photon and electron beam) is implemented, the system developed provides prospective possibilities of performing a wide range of experiments with photon beams for which high luminosity is required, and, in particular, it will essentially simplify and reduce the time requirements and systematic uncertainties of the experiment for the measurement of the polarized proton [8].

References

1. J. Napolitano *et al.*, Phys. Rev. Lett. **61**, 2530 (1988).
2. D. H. Potterveld *et al.*, unpublished (1992).
3. V. A. Matveev, R. M. Muradyan, A. V. Tavkhelidze, Lett. Nuovo Cim. **7**, 719, (1973).
4. S. J. Brodsky, G. R. Farrar, Phys. Rev. Lett. **31**, 1153 (1973).
5. S. J. Brodsky, G. R. Farrar, Phys. Rev. D **11**, 1309 (1975).
6. S. J. Brodsky, J. R. Hiller, Phys. Rev. C **28**, 475 (1983).
7. R. J. Holt *et al.*, CEBAF proposal 89-012 (1989).
8. R. Gilman *et al.*, CEBAF proposal 89-019 (1989).
9. S. I. Nagornij, Ju. A. Kasatkin, I. K. Kirichenko, Nucl. Phys. (russian) **55**, 345,(1992).
10. T. S. H. Lee, Proceedings of the International Conference on Medium and High–Energy Nuclear Physics, Taipei, Taiwan, 23-27 May 1988.

11. Y. Kang *et al.*, Program of the Particles and Nuclei Conference, MIT, Cambridge, MA, p. 1-40, 1990.
12. F. Gross, B. D. Keister, Phys. Rev. C **28**, 823 (1983).
13. V. Burkert *et al.*, Deutron Photodisintegration, CEBAF Letter of Intent, 1988.
14. F. V. Adamian *et al.*, J. Phys. C: Nucl. Phys. **17**, 1657 (1991).
15. V. G. Gorbenko *et al.*, Nucl. Phys. (russian) **35**, 1073 (1982).
16. C. S. Sapp, A. Saha, CEBAF Report, (1990).
17. W. Lotz *et al.*, Nucl. Inst. Meth. B **48**, 256, (1990).
18. J. W. Lightbody, *et al.*, Computers in Physics, May/June, p. 57 (1988).
19. LEGS Progress Report (June 92).
20. V. B. Ganenko *et al.*, Nucl. Phys. 23, 162 (1976).
21. A. A. Beljaev *et al.*, Nucl. Phys. 35, 401 (1982).

Table 1 Kinematics for the measurements.

E_γ GeV	θ_p^{lab} deg	P_p GeV/c	T_p GeV	$d\sigma/d\Omega_p^{Lab}$ nb/sr
		$\theta_p^{cm} = 30°$		
0.6	21.1	1.038	0.461	837.0
0.8	20.1	1.261	0.634	309.0
1.0	19.1	1.475	0.810	135.0
1.2	18.4	1.682	0.988	57.7
1.4	17.7	1.885	1.168	27.3
1.6	17.1	2.086	1.349	17.5
1.8	16.5	2.284	1.531	12.5
2.0	16.0	2.480	1.713	6.6
2.2	15.6	2.675	1.896	4.2
2.4	15.2	2.869	2.080	3.0
		$\theta_p^{cm} = 90°$		
E_γ GeV	θ_p^{lab} deg	P_p GeV/c	T_p GeV	$d\sigma/d\Omega_p^{Lab}$ nb/sr
0.6	68.2	0.806	0.299	660.0
0.8	65.2	0.953	0.399	228.0
1.0	62.7	1.089	0.499	80.0
1.2	60.5	1.218	0.599	21.0
1.4	58.6	1.342	0.699	8.3
1.6	56.8	1.462	0.799	3.0
1.8	55.3	1.580	0.899	1.6
2.0	53.9	2.695	0.999	0.8
2.2	52.5	1.808	1.099	0.4
2.4	51.3	1.920	1.199	0.2
		$\theta_p^{cm} = 150°$		
E_γ GeV	θ_p^{lab} deg	P_p GeV/c	T_p GeV	$d\sigma/d\Omega_p^{Lab}$ nb/sr
0.6	134.5	0.525	0.137	152.0
0.8	131.7	0.579	0.164	46.3
1.0	129.1	0.624	0.188	13.9
1.2	126.8	0.662	0.210	7.8
1.4	124.7	0.697	0.230	3.5
1.6	122.8	0.728	0.249	1.8
1.8	121.0	0.757	0.268	0.8
2.0	119.3	0.785	0.285	0.4
2.2	117.2	0.811	0.302	0.2
2.4	116.2	0.836	0.301	0.1

Table 2 Count rates in the proton arm (Variant A).

$\theta_p^{cm} = 90°$, for Al target walls

E_γ GeV	I_e μA	$(\gamma,p)X$ s^{-1}	$(e,p)X$ s^{-1}	$(\gamma,\pi)X$ s^{-1}	$(e,\pi)X$ s^{-1}
0.6	1	1.60	7.60	1.26	3.38
0.8	1	0.49	3.40	0.33	0.92
1.0	3	0.62	5.50	0.23	0.62
1.2	3	0.26	3.00	0.02	0.05
1.4	5	0.22	0.28	-	-
1.6	5	0.10	1.60	-	-
1.8	5	0.06	0.90	-	-
2.0	5	0.04	0.60	-	-

$\theta_p^{cm} = 90°$, for deuterium

E_γ GeV	I_e μA	$(\gamma,p)n$ amor s^{-1}	$(\gamma,p)n$ crys s^{-1}	$(e,p)X$ s^{-1}	$(\gamma,\pi)X$ amor s^{-1}	$(e,\pi)X$ s^{-1}	total $\pi+p$ amor s^{-1}	total p amor s^{-1}	total p crys s^{-1}
0.6	1	68	214	130	80	207	499	207	353
0.8	1	23	67	70	21	57	176	97	141
1.0	3	23	62	118	15	38	200	146	186
1.2	3	6	14	92	1	4	106	101	109
1.4	3	4	8	72	-	-	78	78	82
1.6	3	1	3	22	-	-	23	23	24
1.8	3	<1	1	11	-	-	12	12	12
2.0	3	<1	<1	7	-	-	7	7	7

$\theta_p^{cm} = 30°$, for deuterium

E_γ GeV	I_e μA	$(\gamma,p)n$ amor s^{-1}	$(\gamma,p)n$ crys s^{-1}	$(\gamma,p)X$ amor k/s	$(e,p)X$ k/s	$(\gamma,\pi)X$ amor k/s	$(e,\pi)X$ k/s	total $\pi+p$ amor k/s	total p amor k/s	total p crys k/s
0.6	1	27	272	5.8	4.0	11.5	5.1	29	10	13
0.8	1	31	90	4.6	3.0	8.1	5.1	21	8	10
1.0	1	13	34	3.5	2.2	5.9	3.5	15	6	7
1.2	2	10	26	5.2	3.2	8.2	4.7	21	8	10
1.4	4	10	22	7.6	4.6	11.5	6.3	30	12	14
1.6	5	8	16	6.9	4.2	9.9	5.2	26	11	12
1.8	5	5	11	5.0	3.1	6.8	3.5	18	8	9
2.0	5	3	6	3.5	2.4	4.5	2.2	13	6	6
2.2	5	2	3	2.8	1.9	3.3	1.4	9	5	5

$\theta_p^{cm} = 150°$, for deuterium

E_γ	I_e	$(\gamma,p)n$	$(\gamma,p)n$	$(\gamma,p)X$	$(e,p)X$	$(\gamma,\pi)X$	$(e,\pi)X$	total $\pi+p$	total p	tot[illegible]
		amor	crys	amor		amor		amor	amor	crys
GeV	μA	s^{-1}	s^{-1}	s^{-1}	s^{-1}	s^{-1}	s^{-1}	k/s	k/s	k/s
0.6	1	15.80	49.50	-	92	-	-	-	107.8	141.5
0.8	1	4.56	13.42	-	56	-	-	-	60.6	69.4
1.0	2	2.63	7.19	-	85	-	-	-	87.6	92.2
1.2	5	3.51	8.77	-	170	-	-	-	173.5	178.8
1.4	5	1.50	3.24	-	142	-	-	-	143.5	145.2
1.6	5	0.72	1.58	-	124	-	-	-	124.7	126.6
1.8	5	0.35	0.70	-	110	-	-	-	110.4	110.7

Table 3 Count rates for neutron arm counter, on deuterium (Variant A).

θ_p^{cm}	θ_n^{Lab}	I_e	$(\gamma,p)X$	$(e,p)X$	$(\gamma,\pi)X$	$(e,\pi)X$	$(\gamma,n)X$	$(e,n)X$	total p,π,n	total n
deg	deg	μA	s^{-1}	s^{-1}	s^{-1}	s^{-1}	s^{-1}	s^{-1}	s^{-1}	s^{-1}
30	133.5	1	-	10.8	3053	529	207	1000	4799	12[illegible]
60	98.2	1	0.4	17.8	1515	2953	178	594	5258	7[illegible]
90	68.2	1	12.6	87	1917	3540	159	333	6049	492
120	44.9	1	399.	449.	4396	5135	183	280	10843	463
150	21.2	1	1546.	1068.	9868	11976	343	304	25107	647

Table 4 Count rates for pn coincidences on deuterium (Variant A).

$\theta_p^{cm} = 30°$

E_γ	I_e	$(\gamma,p)n$ amor	$(\gamma,p)n$ crys	$(e,p)n$	total pn amor true	total pn crys true	amor ratio $\frac{(\gamma,p)}{(e,p)}$	crys ratio $\frac{(\gamma,p)}{(e,p)}$	accid
GeV	μA	s^{-1}	s^{-1}	s^{-1}	s^{-1}	s^{-1}			$10^{-2}/s$
0.6	1	9.89	31.0	21.98	31.07	52.90	0.45	1.01	1.70
0.8	1	3.50	10.3	7.78	11.28	18.08	0.45	1.32	3.70
1.0	1	1.46	3.86	3.32	4.78	7.18	0.44	1.17	8.20
1.2	2	1.19	2.99	2.70	3.89	5.69	0.44	1.10	8.20
1.4	4	1.08	2.35	2.51	3.59	4.86	0.43	0.93	23.7
1.6	5	0.87	1.83	2.02	2.89	3.85	0.43	0.91	26.7
1.8	5	0.62	1.28	1.44	2.06	2.72	0.43	0.89	19.5
2.0	5	0.32	0.64	0.74	1.06	1.38	0.43	0.86	14.1
2.2	5	0.20	0.34	0.47	0.67	0.81	0.43	0.73	11.2

$\theta_p^{cm} = 90°$

E_γ	I_e	$(\gamma,p)n$ amor	$(\gamma,p)n$ crys	$(e,p)n$	total pn amor true	total pn crys true	amor ratio $\frac{(\gamma,p)}{(e,p)}$	crys ratio $\frac{(\gamma,p)}{(e,p)}$	accid
GeV	μA	s^{-1}	s^{-1}	s^{-1}	s^{-1}	s^{-1}			$10^{-2}/s$
0.6	1	7.80	24.5	19.0	26.8	43.6	0.41	1.29	0.063
0.8	1	2.58	7.58	6.61	9.19	14.2	0.39	1.15	0.030
1.0	3	2.59	7.10	7.19	9.78	14.3	0.36	0.98	0.134
1.2	3	0.65	1.63	1.91	2.28	3.54	0.34	0.85	0.093
1.4	5	0.41	0.90	1.28	1.69	2.18	0.32	0.70	0.119
1.6	5	0.15	0.31	0.50	0.65	0.81	0.30	0.62	0.037
1.8	5	0.08	0.16	0.28	0.36	0.44	0.29	0.56	0.020
2.0	5	0.04	0.08	0.13	0.18	0.21	0.28	0.53	0.012

$\theta_p^{cm} = 150°$

E_γ	I_e	$(\gamma,p)n$ amor	$(\gamma,p)n$ crys	$(e,p)n$	total pn amor true	total pn crys true	amor ratio $\frac{(\gamma,p)}{(e,p)}$	crys ratio $\frac{(\gamma,p)}{(e,p)}$	accid
GeV	μA	s^{-1}	s^{-1}	s^{-1}	s^{-1}	s^{-1}			$10^{-2}/s$
0.6	1	1.80	5.64	7.20	9.00	12.8	0.25	0.77	0.031
0.8	1	0.52	1.53	2.26	2.78	3.79	0.23	0.68	0.017
1.0	2	0.30	0.82	1.43	1.73	2.25	0.21	0.58	0.047
1.2	5	0.40	1.00	2.00	2.40	3.00	0.20	0.50	0.230
1.4	5	0.17	0.37	1.13	1.30	1.50	0.15	0.31	0.190
1.6	5	0.09	0.18	0.49	0.58	0.67	0.18	0.37	0.160
1.8	5	0.04	0.08	0.24	0.55	0.63	0.17	0.33	0.570

Table 5 Statistics and beam time (Variant A).

$\theta_p^{cm} = 30°$

E_γ GeV	I_e μA	P_γ	$\Delta\Sigma$	$C_\parallel + C_\perp$ counts	C_a counts	C_e counts	acc/trues %	T hours
0.6	1	0.59	0.05	4510	642	941	1.30	0.04
0.8	1	0.56	0.05	5270	640	1138	3.30	0.14
1.0	1	0.53	0.05	6444	562	1473	6.30	0.41
1.2	2	0.50	0.05	7800	658	1861	25.0	0.62
1.4	4	0.47	0.05	10236	662	2632	83.0	0.93
1.6	5	0.45	0.05	11586	664	3026	124.	1.32
1.8	5	0.40	0.05	15686	673	4228	127.	2.51
2.0	5	0.35	0.05	21823	679	6029	125.	6.83
2.2	5	0.30	0.05	33848	690	9609	167.	17.37
							total	30.17

$\theta_p^{cm} = 90°$

E_γ GeV	I_e μA	P_γ	$\Delta\Sigma$	$C_\parallel + C_\perp$ counts	C_a counts	C_e counts	acc/trues %	T hours
0.6	1	0.59	0.05	4882	728	1070	0.017	0.06
0.8	1	0.56	0.05	6190	1944	1455	0.025	0.24
1.0	3	0.53	0.05	7964	1654	2021	0.110	0.28
1.2	3	0.50	0.05	10206	979	2758	0.320	1.32
1.4	5	0.47	0.05	14548	1100	4304	0.660	2.97
1.6	5	0.45	0.05	18222	1229	5624	0.550	9.90
1.8	5	0.40	0.05	25438	1285	8101	0.560	25.62
2.0	5	0.35	0.10	8892	1335	2887	1.280	19.72
							total	60.11

$\theta_p^{cm} = 150°$

E_γ GeV	I_e μA	P_γ	$\Delta\Sigma$	$C_\parallel + C_\perp$ counts	C_a counts	C_e counts	acc/trues %	T hours
0.6	1	0.59	0.05	8094	1647	2291	0.017	0.31
0.8	1	0.56	0.05	10288	1832	3056	0.026	1.31
1.0	2	0.53	0.05	13934	2104	4396	0.130	2.91
1.2	5	0.50	0.05	19195	2367	6400	0.440	2.94
1.4	5	0.47	0.05	40120	3988	15141	0.657	12.00
1.6	5	0.45	0.05	36100	2962	13171	1.230	23.85
1.8	5	0.40	0.10	13595	3251	5115	2.260	21.32
							total	64.64

Table 6 Count rates in the proton arm, for deuterium (Variant B).

$\theta_p^{cm} = 30°$

E_γ	I_e	total $\pi + p$ amor	total p amor	total p crys
GeV	μA	s^{-1}	s^{-1}	s^{-1}
0.6	1	1442	482	623
0.8	1	1059	382	493
1.0	3	784	295	382
1.2	4	1115	435	538
1.4	10	1593	637	748
1.6	10	1396	575	611
1.8	15	984	415	440
2.0	20	669	293	311
2.2	30	508	231	246

$\theta_p^{cm} = 90°$

E_γ	I_e	total $\pi + p$ amor	total p amor	total p crys
GeV	μA	s^{-1}	s^{-1}	s^{-1}
0.6	1	12.40	5.70	26.70
0.8	1	3.70	1.88	8.30
1.0	3	3.11	1.89	7.30
1.2	6	1.20	0.96	3.18
1.4	10	0.60	0.60	1.72
1.6	20	0.44	0.44	1.04
1.8	30	0.36	0.36	0.72
2.0	30	0.17	0.17	0.33
2.2	30	0.08	0.08	0.14

$\theta_p^{cm} = 150°$

E_γ	I_e	total $\pi + p$ amor	total p amor	total p crys
GeV	μA	s^{-1}	s^{-1}	s^{-1}
0.6	1	1.32	1.32	6.20
0.8	3	1.14	1.14	5.03
1.0	5	0.55	0.55	2.10
1.2	10	0.58	0.58	1.94
1.4	20	0.50	0.50	1.43
1.6	30	0.38	0.38	0.93
1.8	30	0.18	0.18	0.38
2.0	30	0.08	0.08	0.16

Table 7 Count rates for neutron arm counter, on deuterium (Variant B).

θ_p^{cm}	θ_n^{Lab}	I_e	$(\gamma,p)X$	$(\gamma,\pi)X$	$(\gamma,n)X$	total	total
					p,π,n	n	
deg	deg	μA	s^{-1}	s^{-1}	s^{-1}	s^{-1}	s^{-1}
30	133.5	1	-	254	17	271	17
60	98.2	1	0.04	126	15	141	15
90	68.2	1	1.05	160	13	173	13
120	44.9	1	33.00	366	15	414	15
150	21.2	1	129.00	822	28	979	28

Table 8 Statistics and beam time (Variant B).

$\theta_p^{cm} = 30°$

E_γ	I_e	P_γ	$\Delta\Sigma$	$(\gamma,p)n)$ amor	$(\gamma,p)n)$ crys	$C_{\|\|} + C_\perp$	C_a	acc/trues	T
GeV	μA			s^{-1}	s^{-1}	counts	counts	%	hours
0.6	1	0.74	0.05	0.82	3.88	974	642	0.06	0.29
0.8	1	0.70	0.05	0.39	1.29	1090	640	0.15	0.85
1.0	3	0.67	0.05	0.35	1.35	1216	662	0.81	0.78
1.2	4	0.62	0.05	0.28	0.88	1389	658	2.12	1.50
1.4	10	0.56	0.05	0.22	0.64	1702	662	8.50	1.57
1.6	10	0.49	0.05	0.14	0.34	2220	664	9.86	3.13
1.8	15	0.42	0.05	0.15	0.31	3025	673	14.7	3.93
2.0	20	0.36	0.05	0.11	0.21	4117	679	18.8	7.31
2.2	30	0.28	0.05	0.10	0.17	5929	690	34.8	11.68
2.4	30	0.22	0.10	0.07	0.11	2135	172	34.2	6.24
								total	37.28

$\theta_p^{cm} = 90°$

E_γ	I_e	P_γ	$\Delta\Sigma$	$(\gamma,p)n)$ amor	$(\gamma,p)n)$ crys	$C_{\|\|} + C_\perp$	C_a	acc/trues	T
GeV	μA			s^{-1}	s^{-1}	counts	counts	%	hours
0.6	1	0.74	0.05	0.65	3.07	974	642	0.001	0.36
0.8	1	0.70	0.05	0.22	0.95	1090	640	0.001	1.12
1.0	3	0.67	0.05	0.22	0.83	1216	662	0.003	1.24
1.2	6	0.62	0.05	0.11	0.36	1389	658	0.006	2.76
1.4	10	0.56	0.05	0.07	0.20	1702	662	0.010	5.12
1.6	20	0.49	0.05	0.05	0.12	2220	664	0.020	8.83
1.8	20	0.42	0.05	0.04	0.08	3025	673	0.030	15.17
2.0	30	0.36	0.07	0.02	0.04	2058	340	0.030	19.80
2.2	30	0.28	0.10	0.01	0.02	1482	171	0.032	31.00
								total	85.40

$\theta_p^{cm} = 150°$

E_γ	I_e	P_γ	$\Delta\Sigma$	$(\gamma,p)n)$ amor	$(\gamma,p)n)$ crys	$C_\parallel + C_\perp$	C_a	acc/trues	T
GeV	μA			s^{-1}	s^{-1}	counts	counts	%	hours
0.6	1	0.74	0.05	0.15	0.71	974	642	0.001	1.57
0.8	3	0.70	0.05	0.13	0.57	1090	640	0.003	1.90
1.0	5	0.67	0.05	0.06	0.24	1216	662	0.005	4.33
1.2	10	0.62	0.05	0.07	0.22	1389	658	0.012	4.51
1.4	20	0.56	0.05	0.06	0.16	1702	662	0.024	6.13
1.6	30	0.49	0.05	0.04	0.11	2220	664	0.036	9.90
1.8	30	0.42	0.10	0.02	0.04	756	168	0.036	7.13
2.0	30	0.36	0.10	0.01	0.02	1029	170	0.035	20.85
								total	56.32

Table 9 Total time of the experiment.

Variant A. Mixed $\gamma + e^-$ beam.
Crystal thickness: 6 mm.
Total time: 365 hours.

C.M. Angle deg	Energy range Gev	I_e muA	T hours
30	$0.6 \rightarrow 2.2$	$1 \rightarrow 5$	84
90	$0.6 \rightarrow 2.0$	$1 \rightarrow 5$	113
150	$0.6 \rightarrow 1.8$	$1 \rightarrow 5$	118
60, 120	1.0, 1.4, 1.8	$1 \rightarrow 5$	50

Variant B. Separate γ and e^- beams.
Crystal thickness: 0.5 mm.
Total time: 390 hours.

C.M. Angle deg	Energy range Gev	I_e muA	T hours
30	$0.6 \rightarrow 2.4$	$1 \rightarrow 30$	90
90	$0.6 \rightarrow 2.2$	$1 \rightarrow 30$	140
150	$0.6 \rightarrow 2.0$	$1 \rightarrow 30$	110
60, 120	1.0, 1.4, 2.0	$1 \rightarrow 30$	50

Variant B. Separate γ and e^- beams.
Crystal thickness: 1.0 mm.
Total time: 273 hours.

C.M. Angle deg	Energy range Gev	I_e muA	T hours
30	$0.6 \rightarrow 2.4$	$1 \rightarrow 30$	71
90	$0.6 \rightarrow 2.2$	$1 \rightarrow 30$	96
150	$0.6 \rightarrow 2.0$	$1 \rightarrow 30$	71
60, 120	1.0, 1.4, 2.0	$1 \rightarrow 30$	25

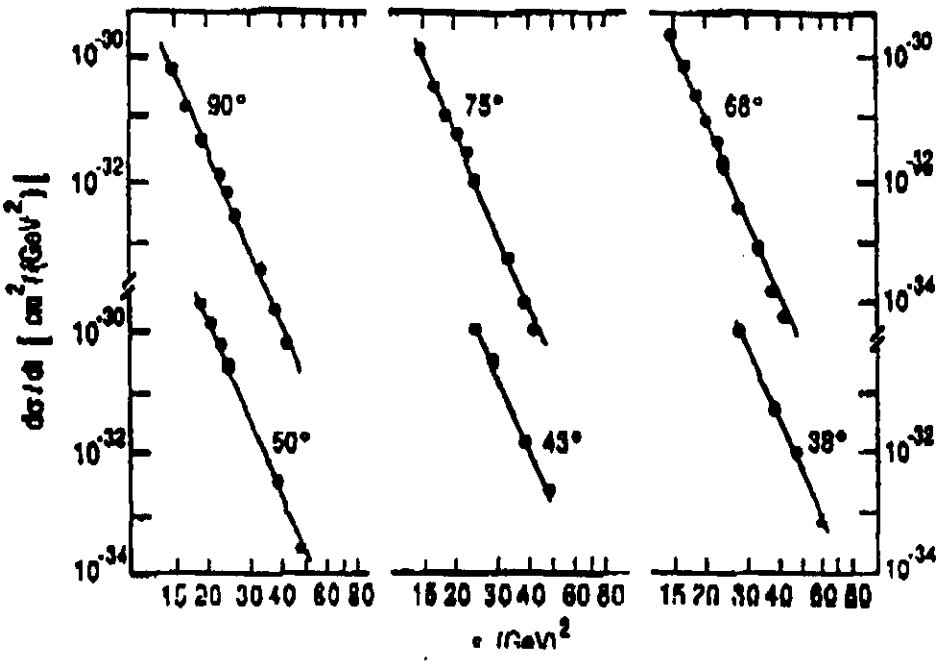

Figure 1a. Elastic proton-proton scattering cross sections, plotted versus the Mandelstam varianle s, for fixed center-of-mass angles.

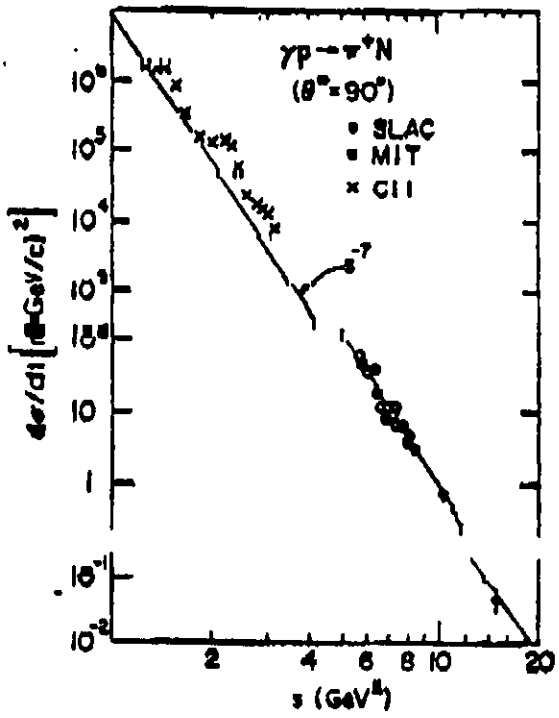

Figure 1b. The cross section for the reaction $\gamma + p \rightarrow \pi^+ + n$ at a fixed center-of-mass angle as a function of the total energy squared s.

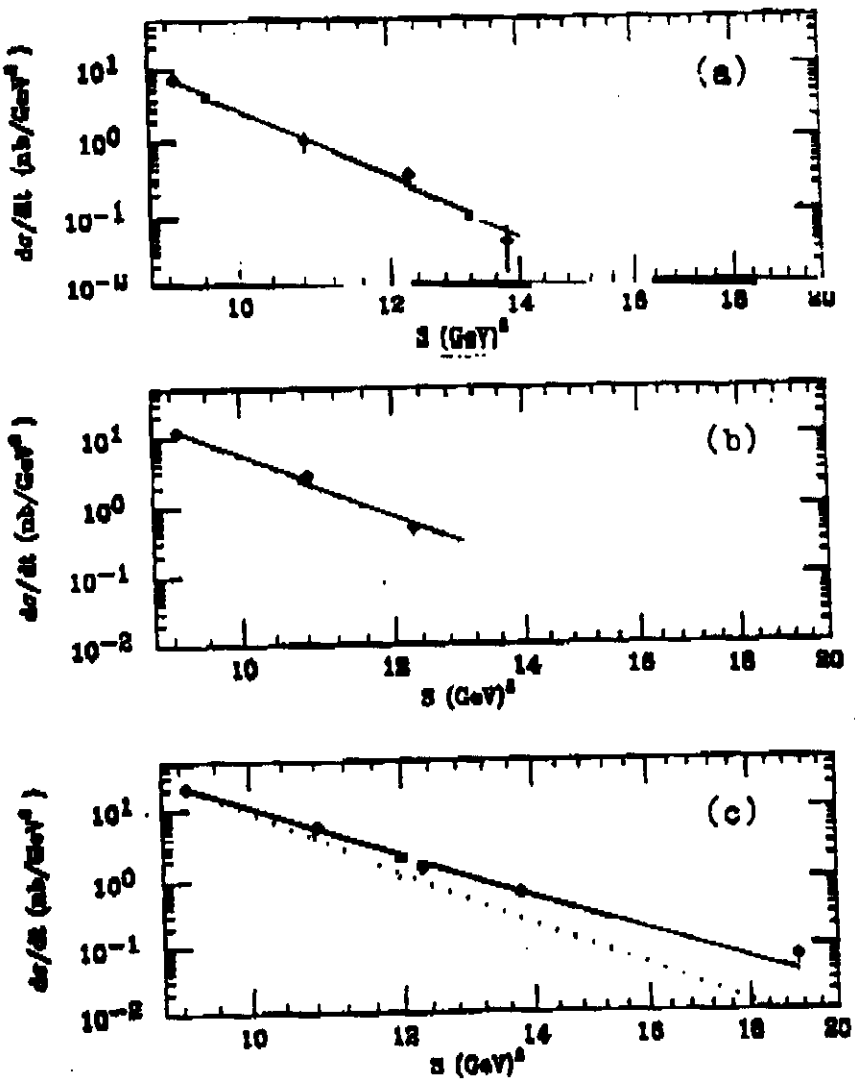

Fig.2. Preliminary cross section data /2/ for the reaction $\gamma d \to p n$ for angles 90° (a), 53° (b) and 37° (c). The lines are a fit to the data of the form $1/s^n$, in which n = 12.1 ± 0.8 (a), 11.0 ± 0.5 (b) and 8.7 ± 0.3 (c) s^{-n} extrapolation on fig.2c is plotted as the dotted line (Fig. from ref. /2/).

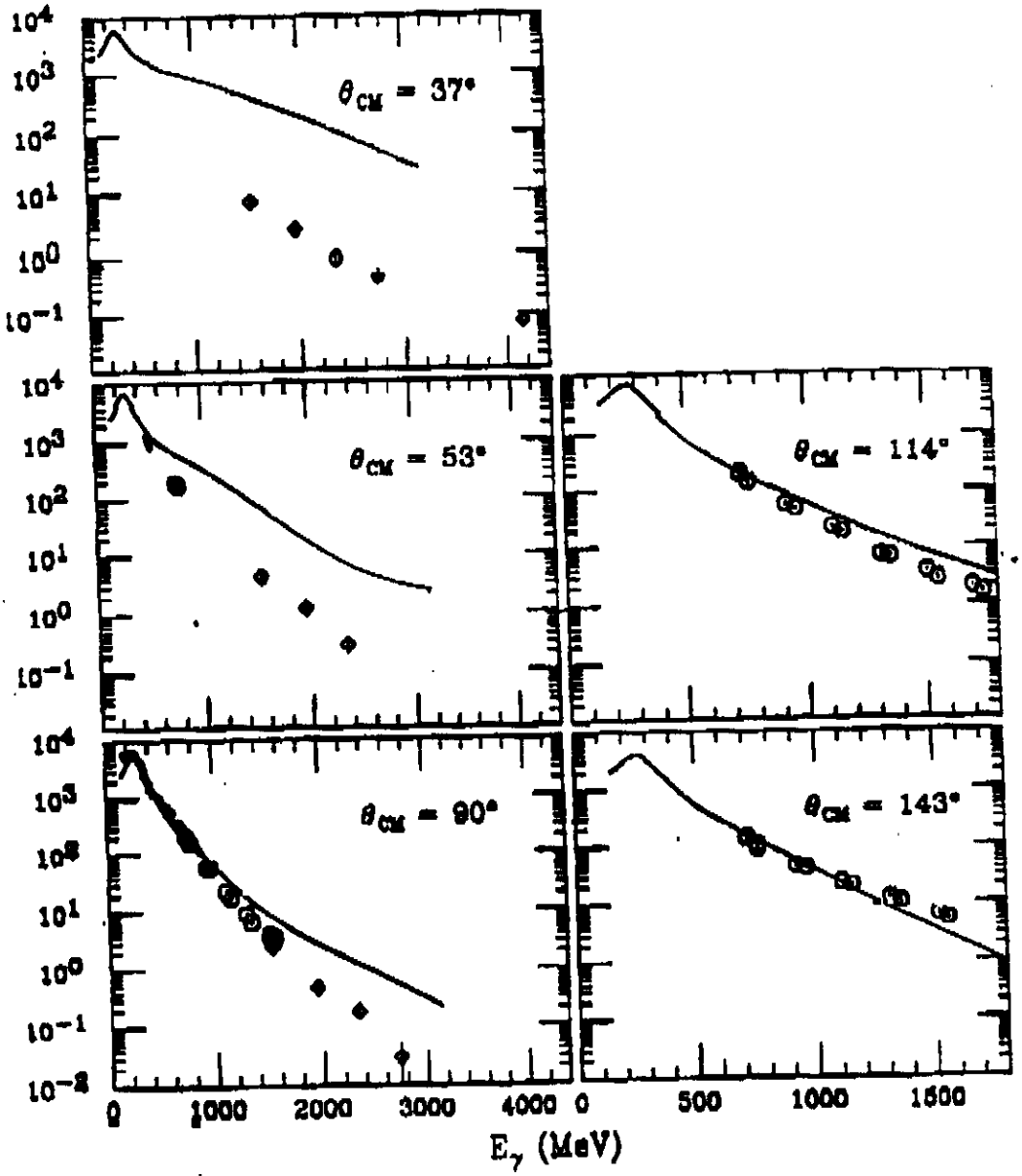

Fig.3. $d\sigma/d\Omega^{cm}$ deuteron photodisintegration cross section in nb/sr for /1/ (circles) and preliminary results /2/ (diamonds). The other data points are from /24-26/. The curves are the calculations /10/ for the Paris potential. (Fig. from ref. /2/).

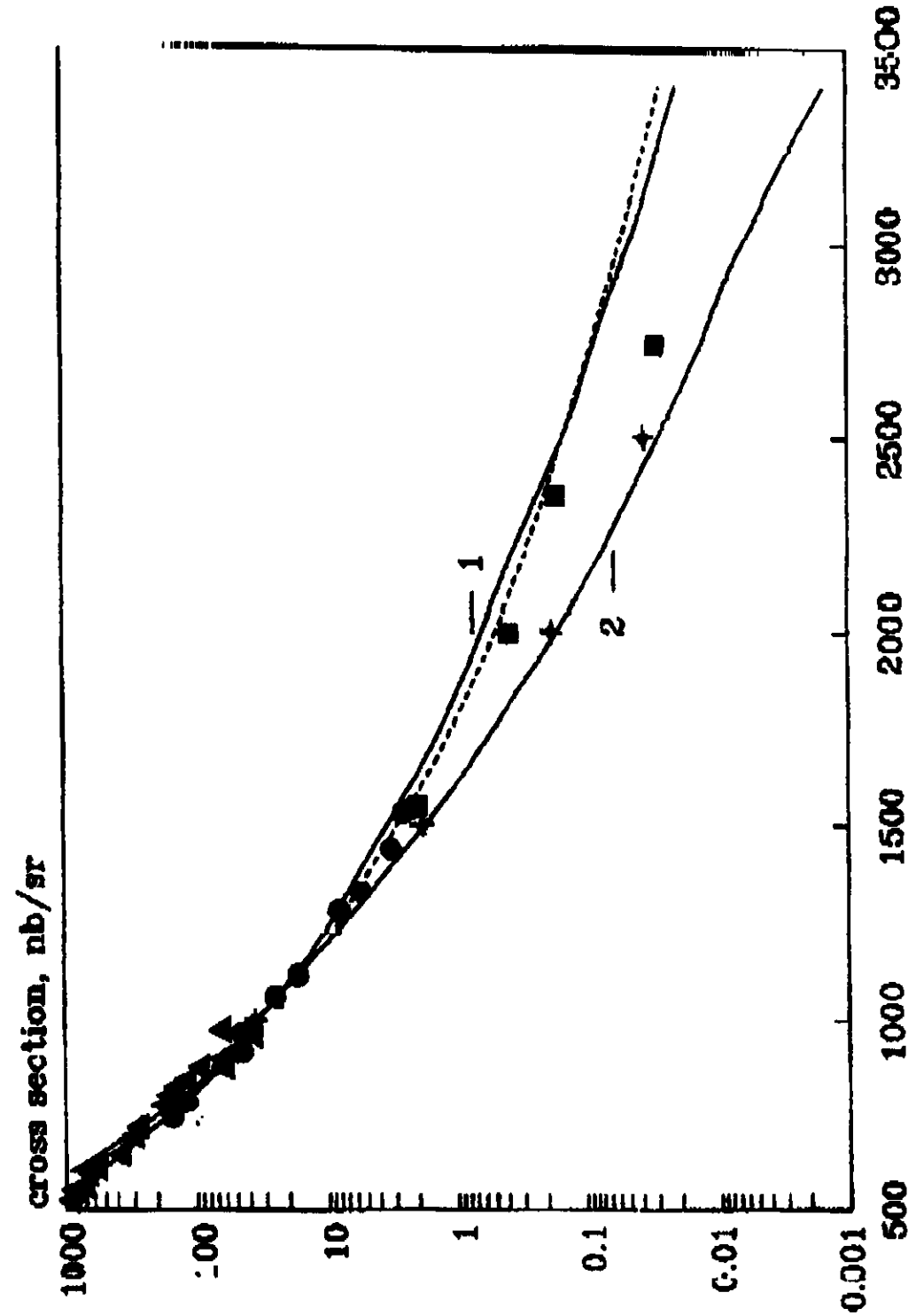

Fig.4a. Deutron photodisintegration cross section at a center-of-mass angle of 90°. The data are from ref. /26/ (▲), /1/ (●) and preliminary data from ref./2/ (■). The curves are a calculation /9/ for $\xi = 3$ (1) and $\xi = 4$ (2) when only NN configurations ($\alpha = 0$) are taken into account, the dashed curve is the calculation /9/ with NN and NN* configurations ($\alpha = 15$) in the deutron wave function. Crosses (+) is the results of the calculation /13/ based on model /6/.

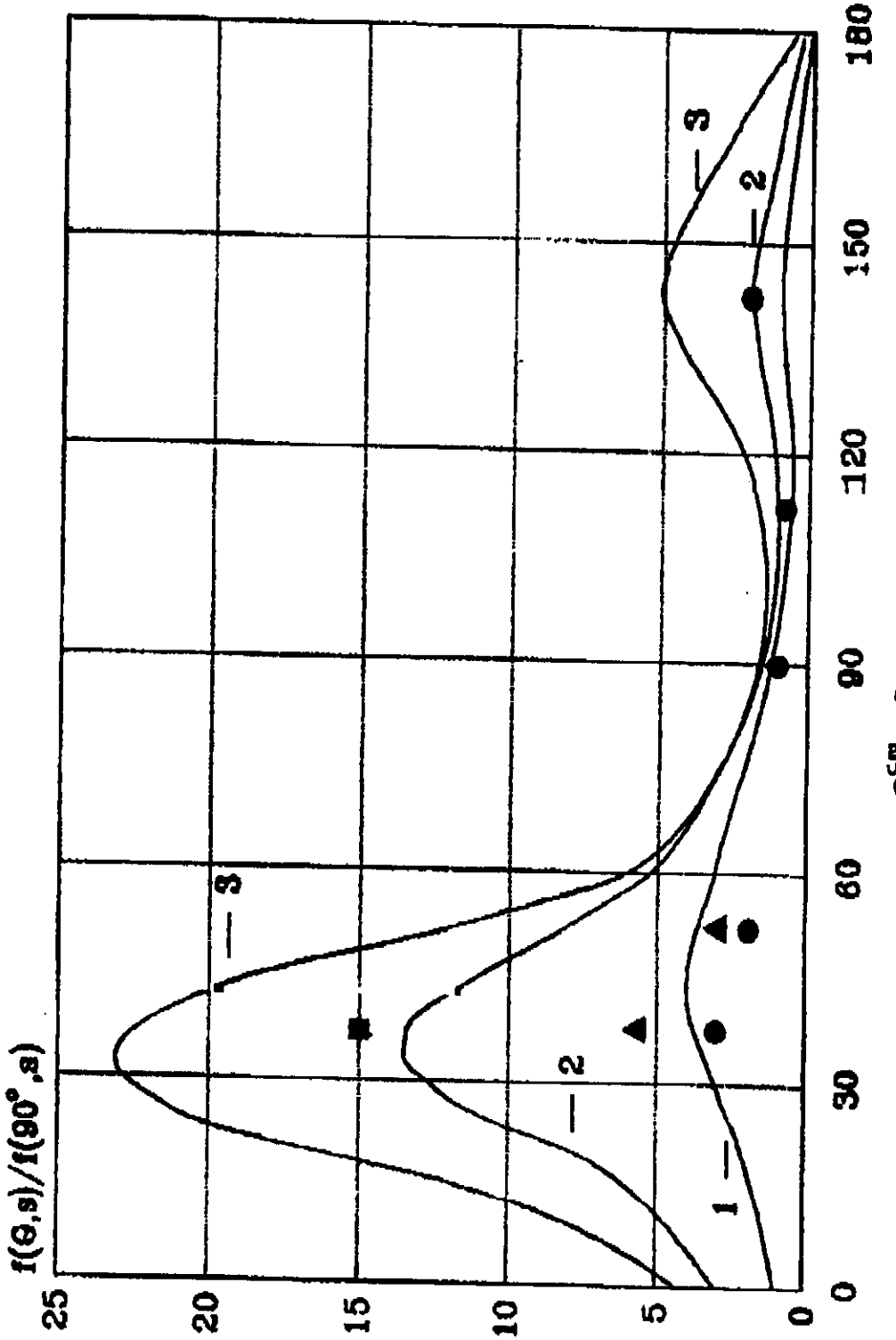

4b. Relative angular distributions of deuteron photodisintegration. Curves are the calculation /9/ for photon energies 1GeV (1), 2 GeV (2) and 3 GeV (3) with only NN configuration in the deuteron wave function. Experimental data are from ref./1,2/ for photon energies 1.5 GeV (●), 2 GeV (▲) and 2.74 GeV (■).

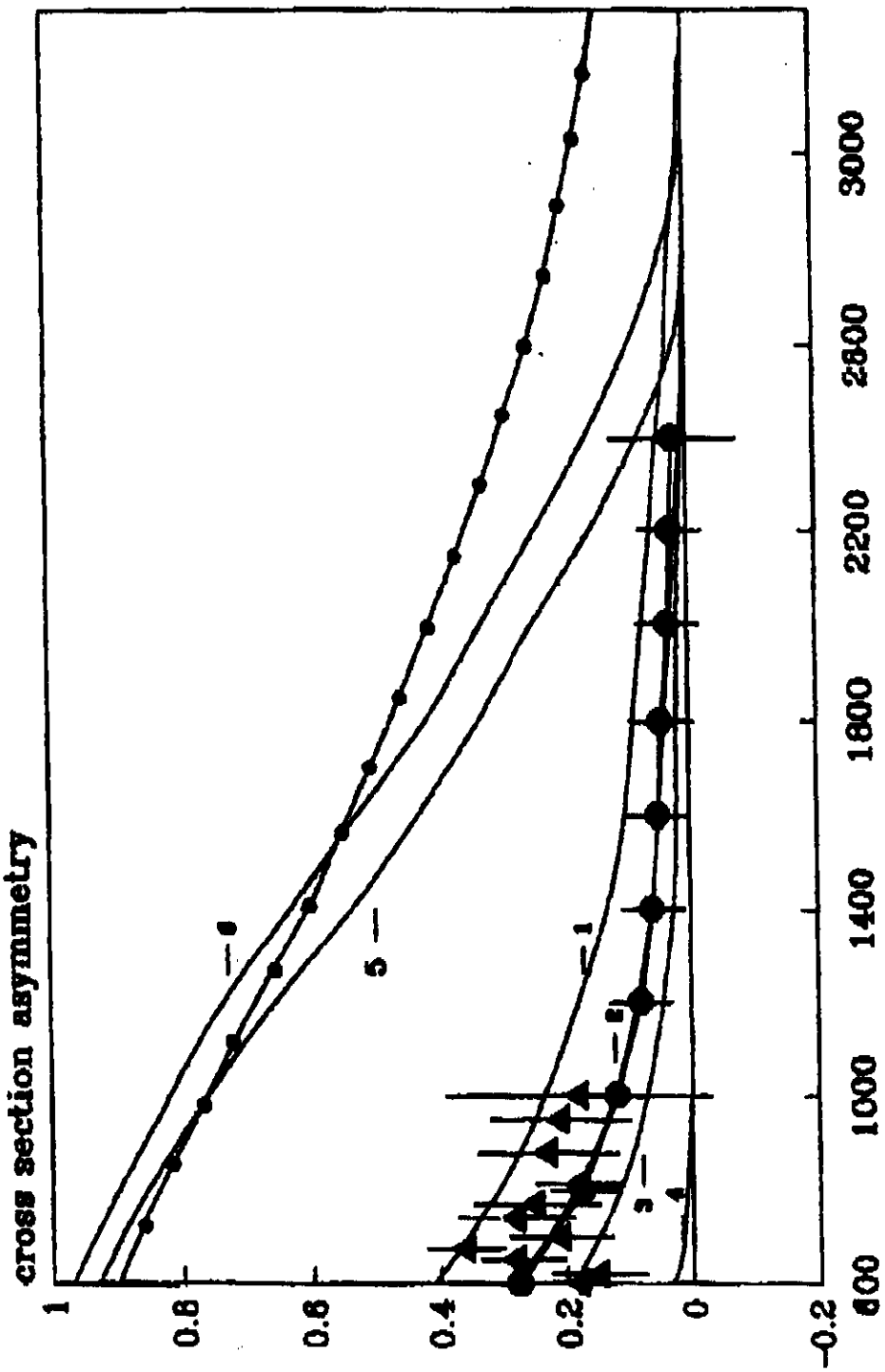

Fig.5a. Energy dependence of the cross section asymmetry at center-of-mass angle of 90° and $\xi_n=3$. The curves are a calculation /9/ with NN configuration ($\alpha = 0$) in the deuteron wave function (—•—•—) and when the NN* configurations are taken into account with $\alpha = 10$, 15 20 and 30 (lines 1, 2, 3, 4 respectively). Curves 5 and 6 are the off shell calculation only with NN configuration. Data from ref./14/ (Δ), circles are the expected results for proposed experiment.

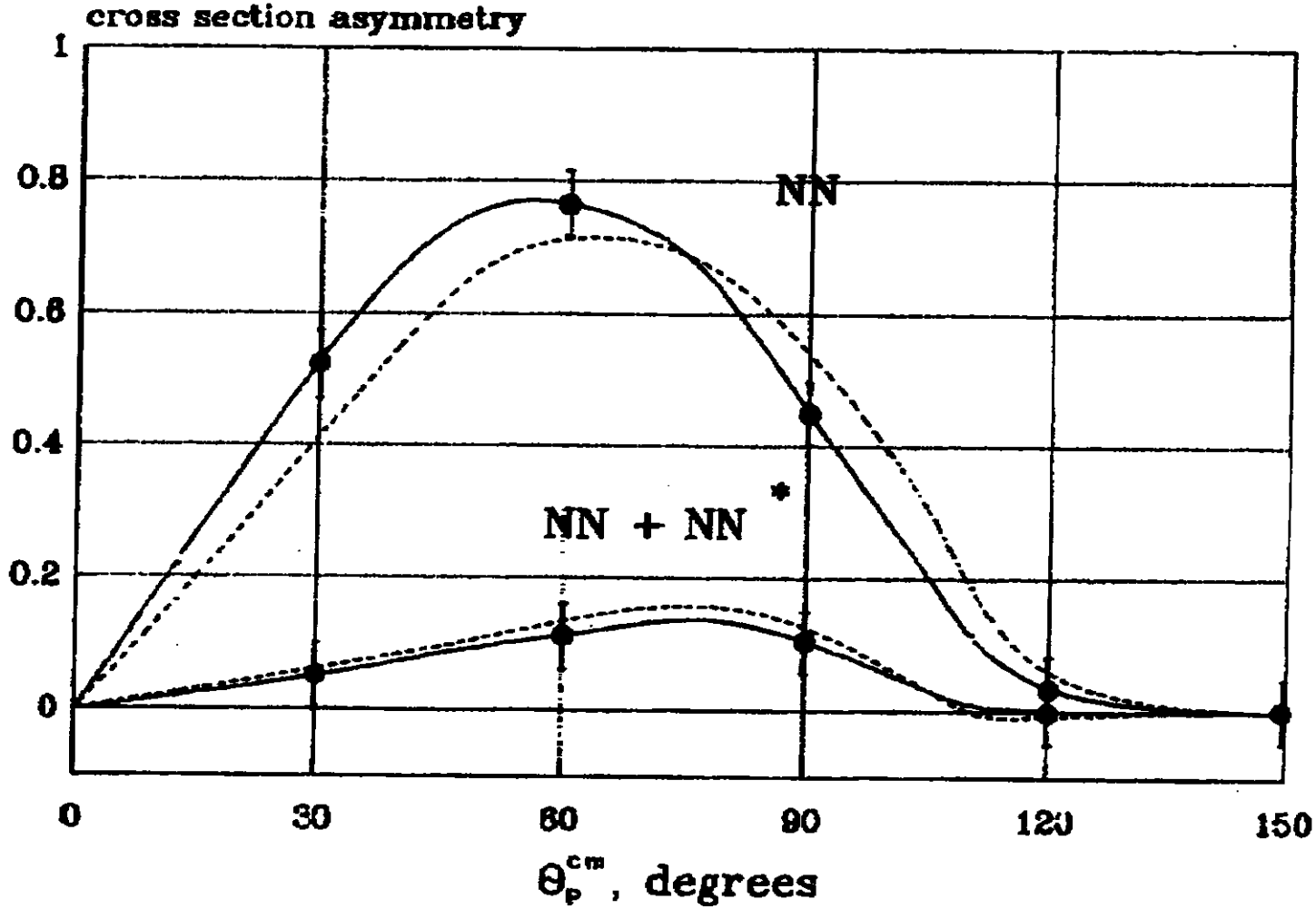

Fig.5b. Angular distribution of the cross section asymmetry of deuteron photodisintegration for E_γ = 1.5 GeV. The curves are off shell (———) and on shell (- - - - -) calculations /9/ when only NN (α = 0) and NN and NN* (α = 10) configurations are taken into account in the deuteron wave function. Circles are the expectable results of the proposed experiment.

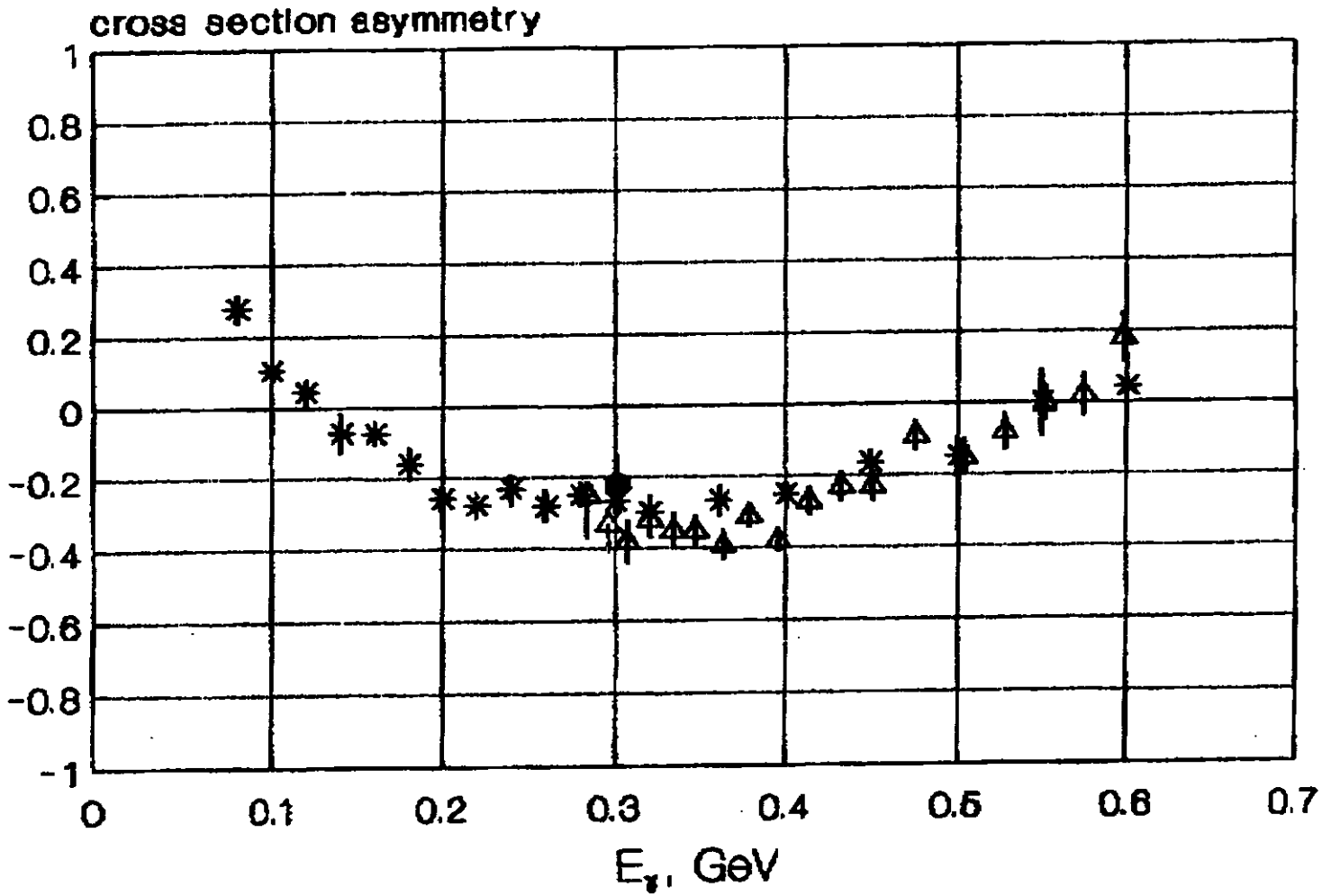

Fi_.5c. Cross section asymmetry of the deuteron photodisintegration at a center-of mass angle of 90°. The data are from ref /14/ (△) and /15/ (✱). (●) - our data, obtained on mixed γ + e^- beam.

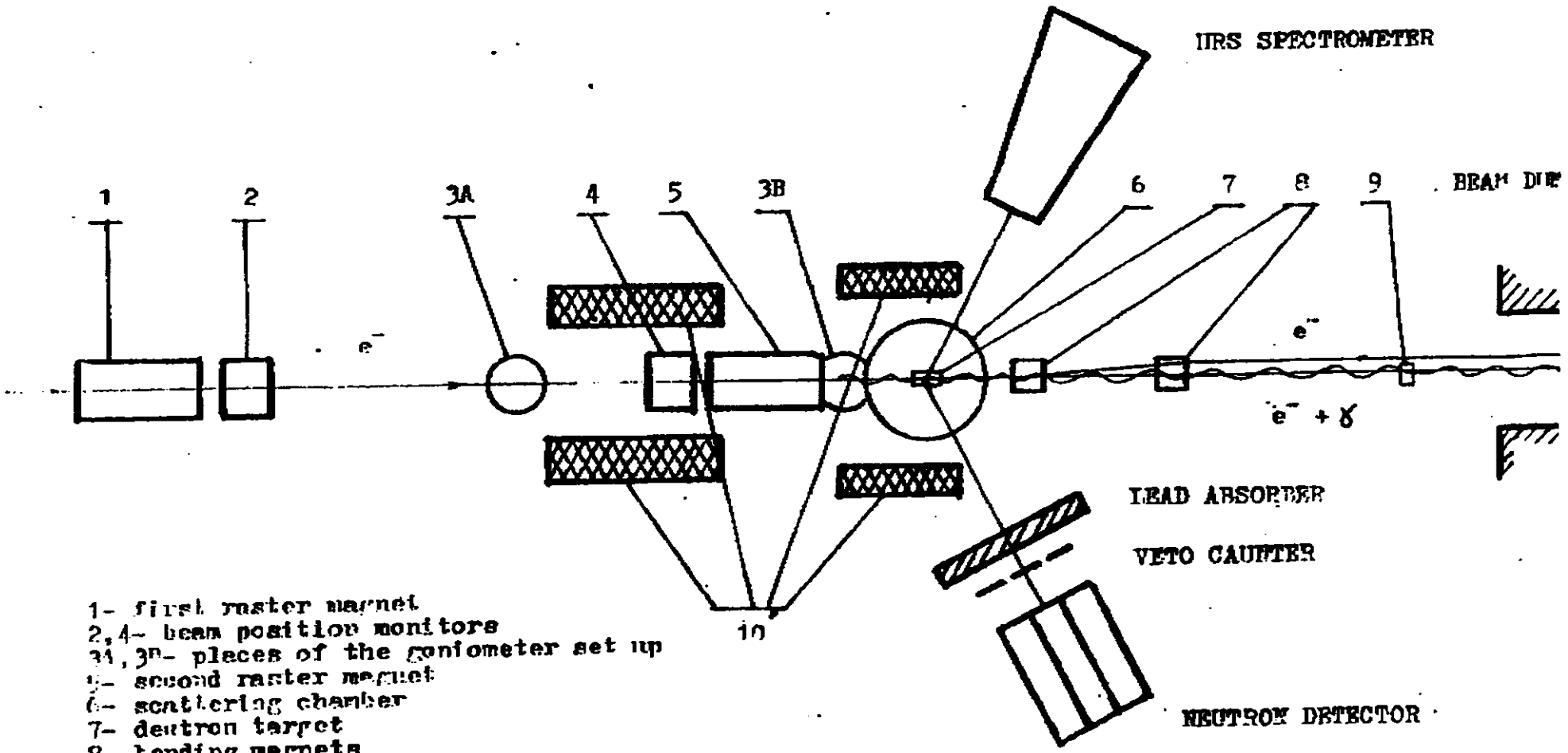

Fig.6. Experimental set up for variant A

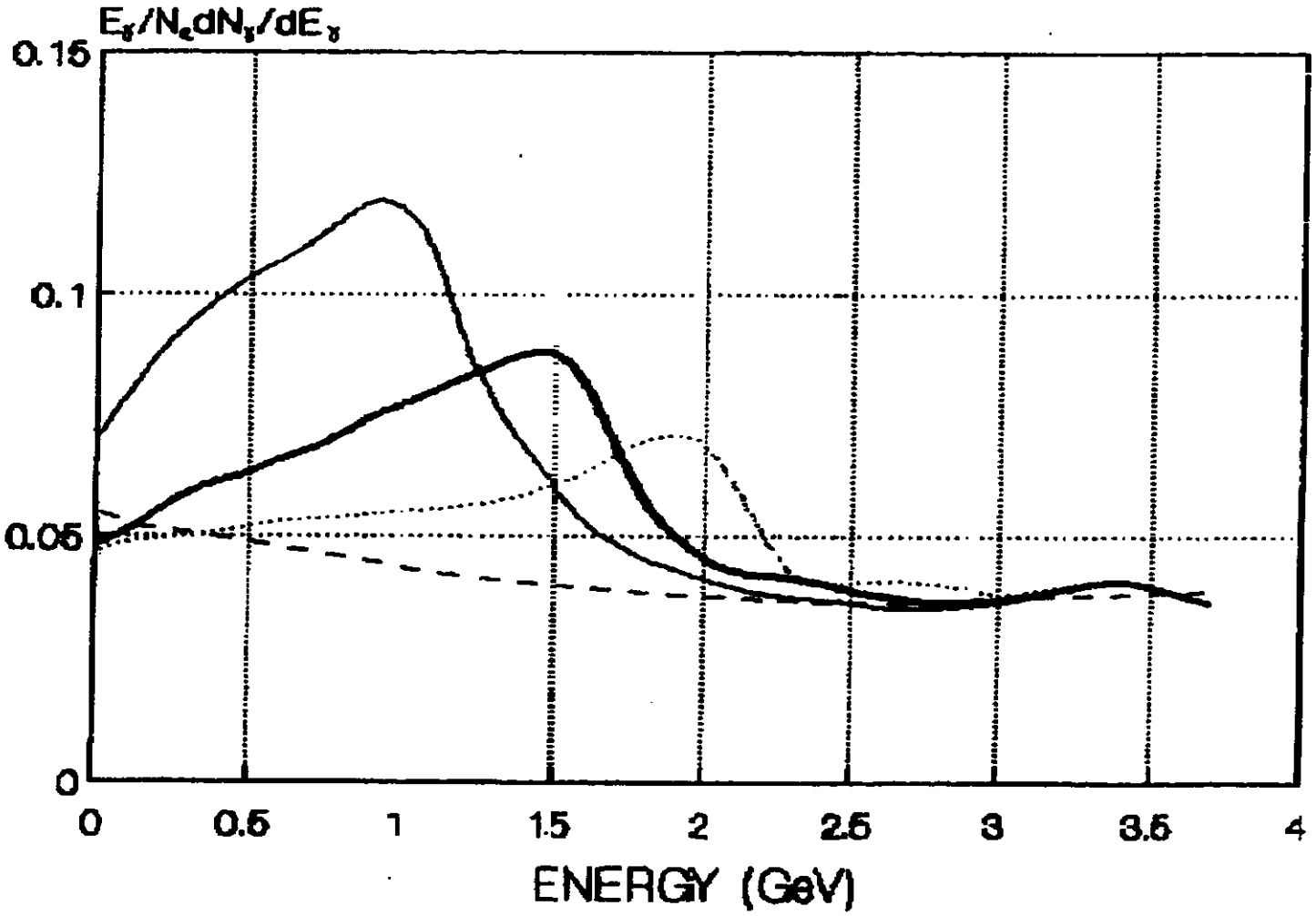

Fig.7a. Spectra of coherent bremsstrahlung for electron energy E_0 = 4 GeV and peak photon energies 1 GeV (——), 1.5 GeV (— — —), 2 GeV (·····). Diamond, orientation (2,2,6), thick 6 mm.– – – –bremsstrahlung spectrum.

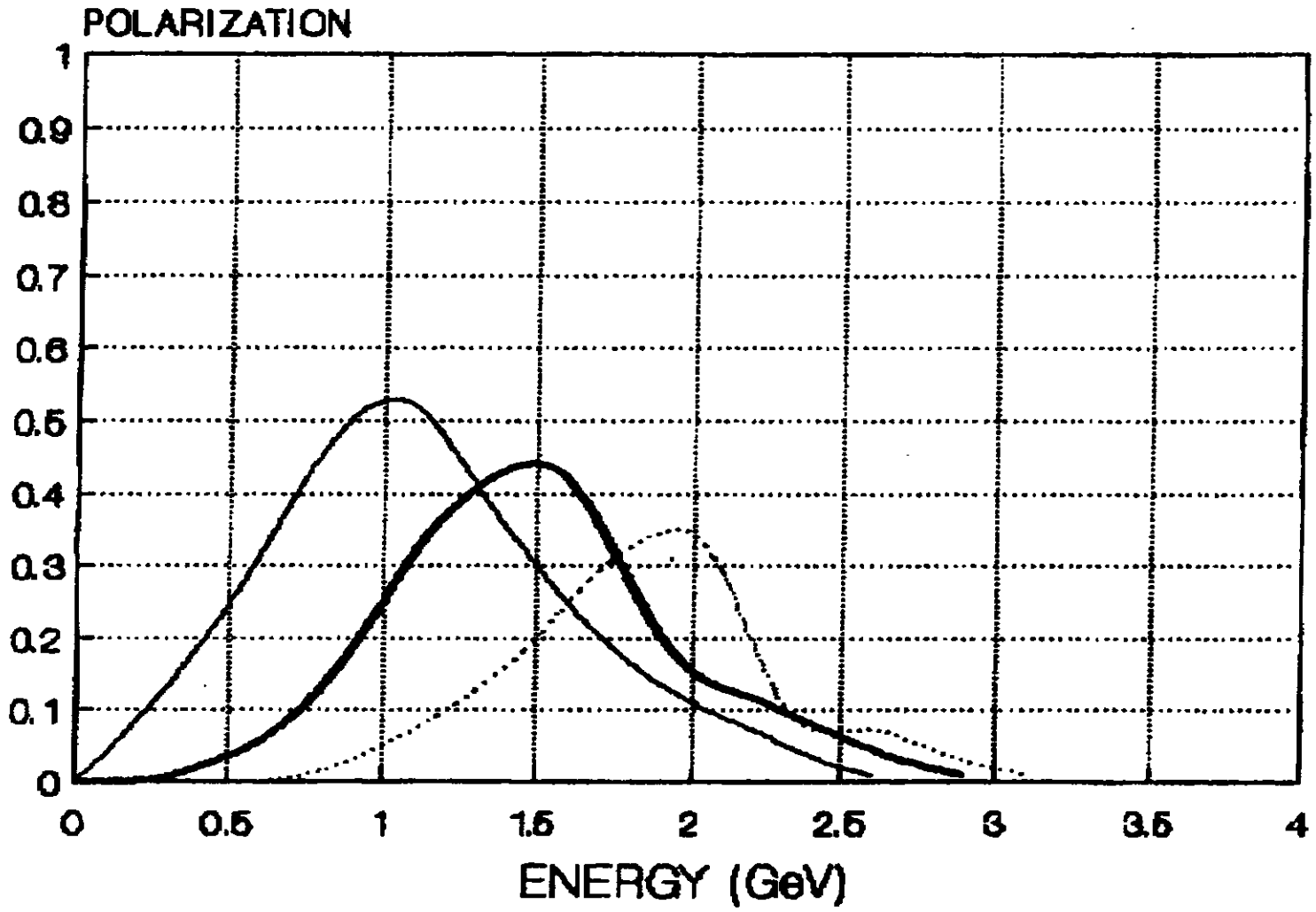

Fig.7a. Polarization of cocherent bremsstrahlung. Notation and conditions the same as in fig.3a.

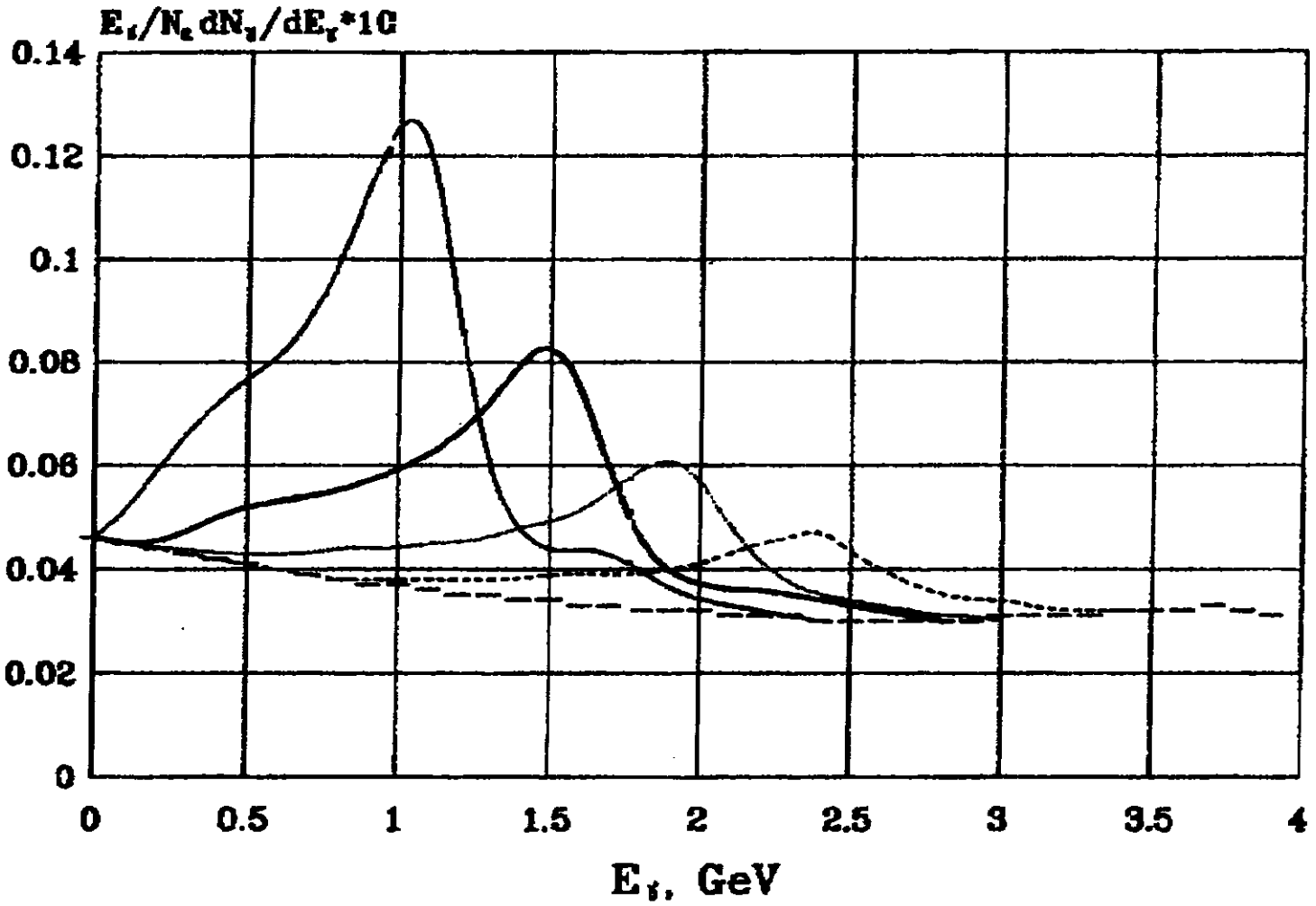

Fig.7c. Spectra of coherent bremsstrahlung for electron energy E_e = 4 GeV and peak photon energies 1.1 GeV (————), 1.5 GeV (————), 2 GeV (·····) and 2.4 GeV (– – – –) Diamond, orientation (2,2,0), thick 0.5 mm (- - - -) bremsstrahlung spectrum.

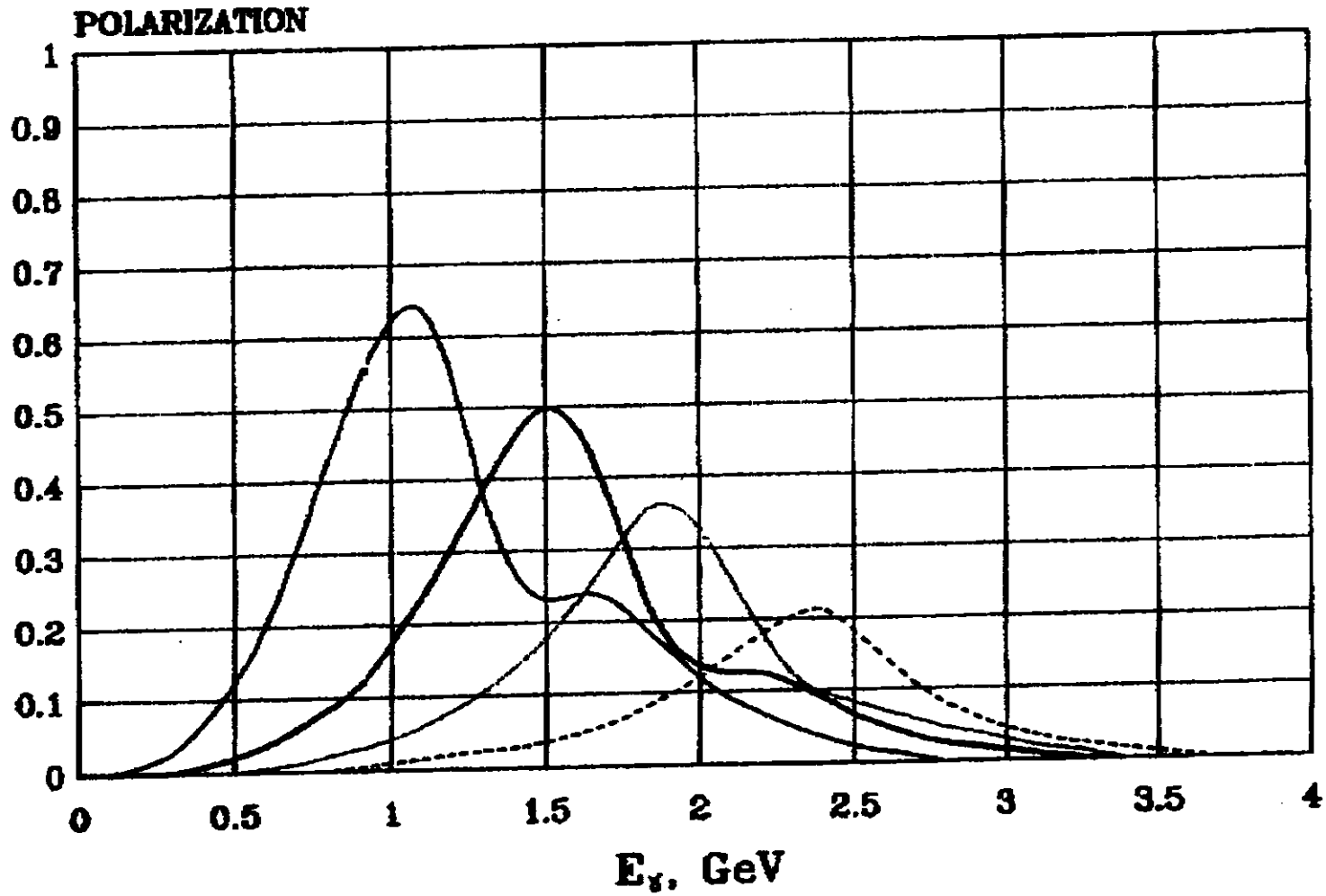

Fig.7d. Polarization of coherent bremsstrachlung. Notations and conditions the same as in fig.7c.

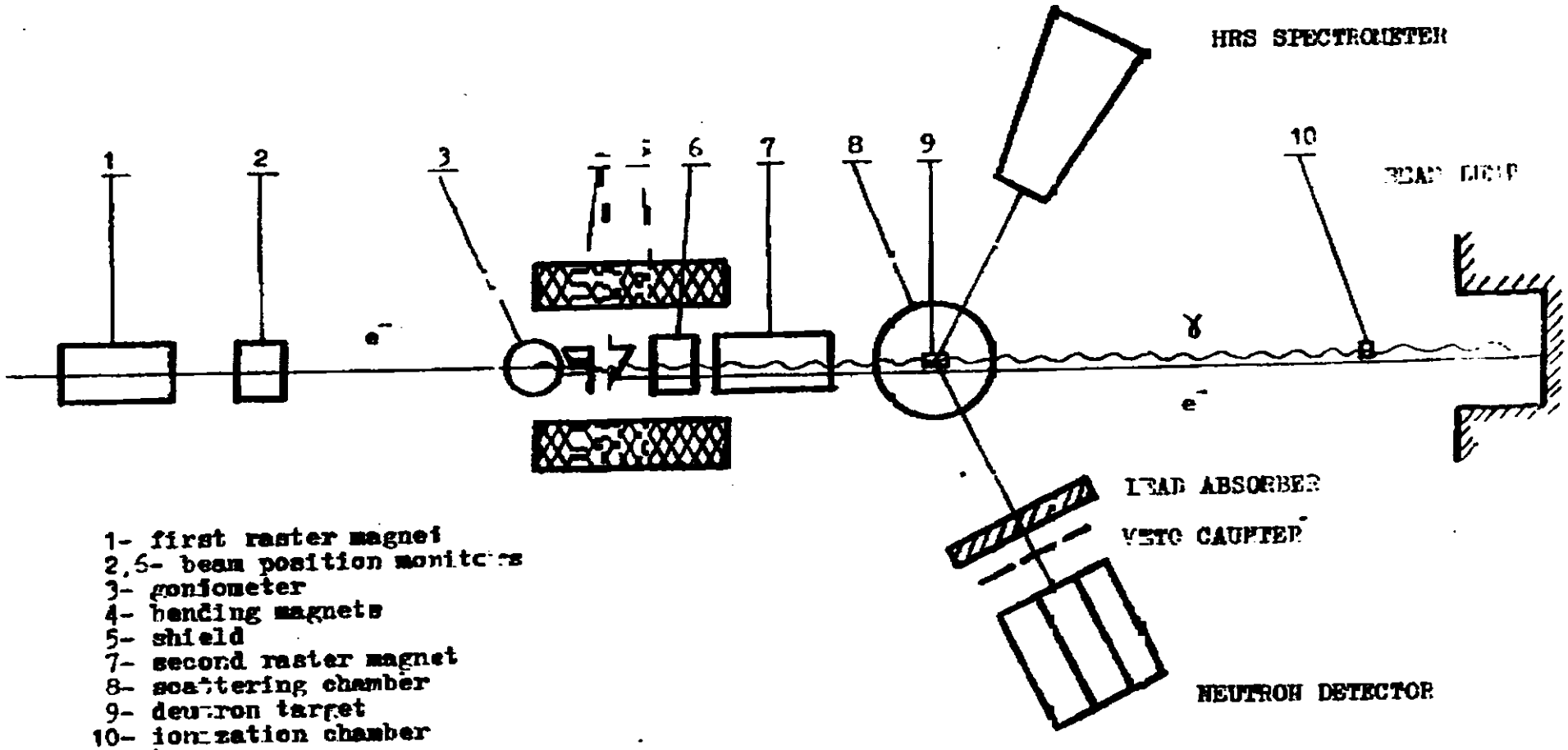

Fig. 3. Experimental set up for variant E

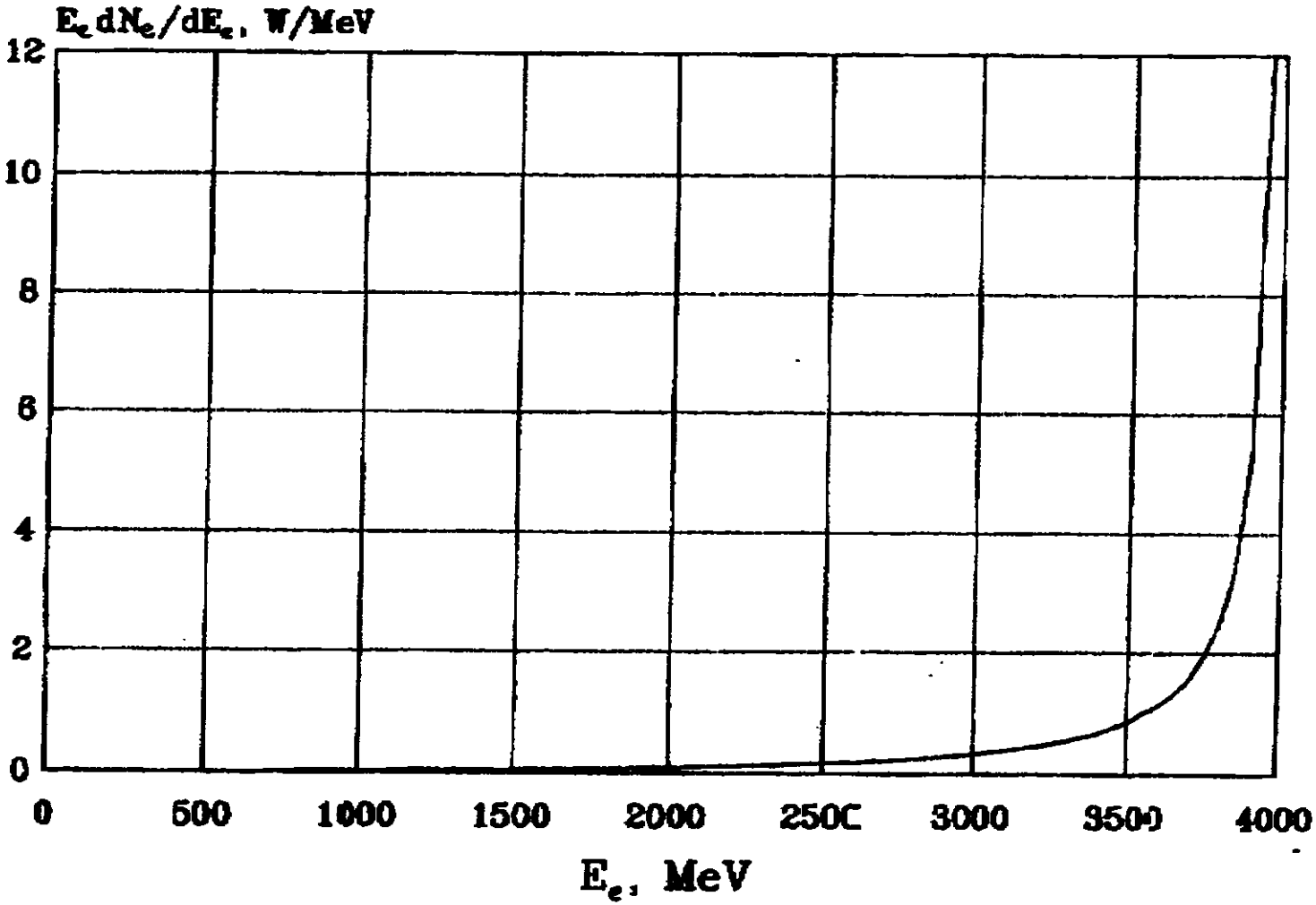

Fig.9. Spectr of the energy of the beam scattered electrons after passing 0.5 mm thick diamond singl crystal.

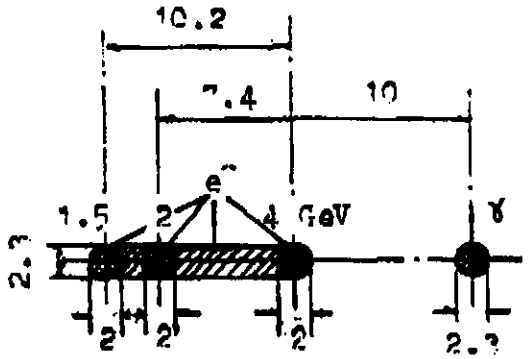

A

on the exit from magnetic system

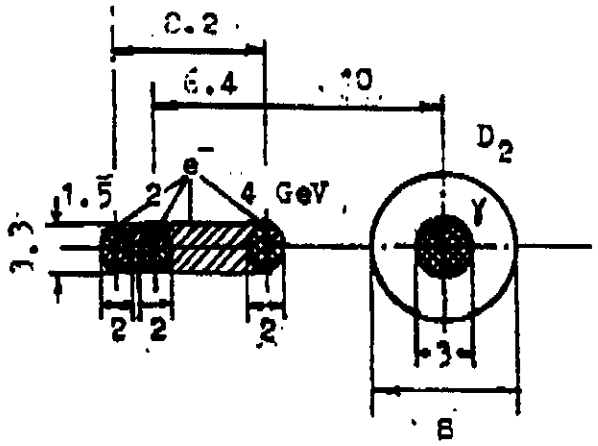

B

in the region of the deutron target

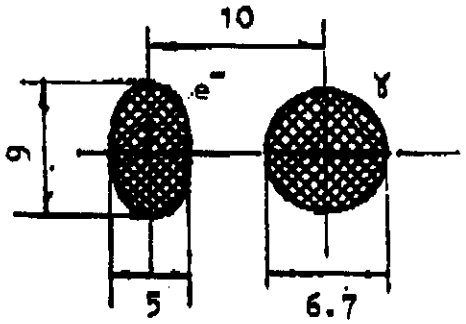

C

on the distance of the 15 m from the magnetic system

Fig.10. Arrangement and sizes of the gamma and electron beams on some places of beam line for the diamond crystal 0.5 mm thick. Size of the electron beam before crystal 2 mm, divergence 0.1 mrad.

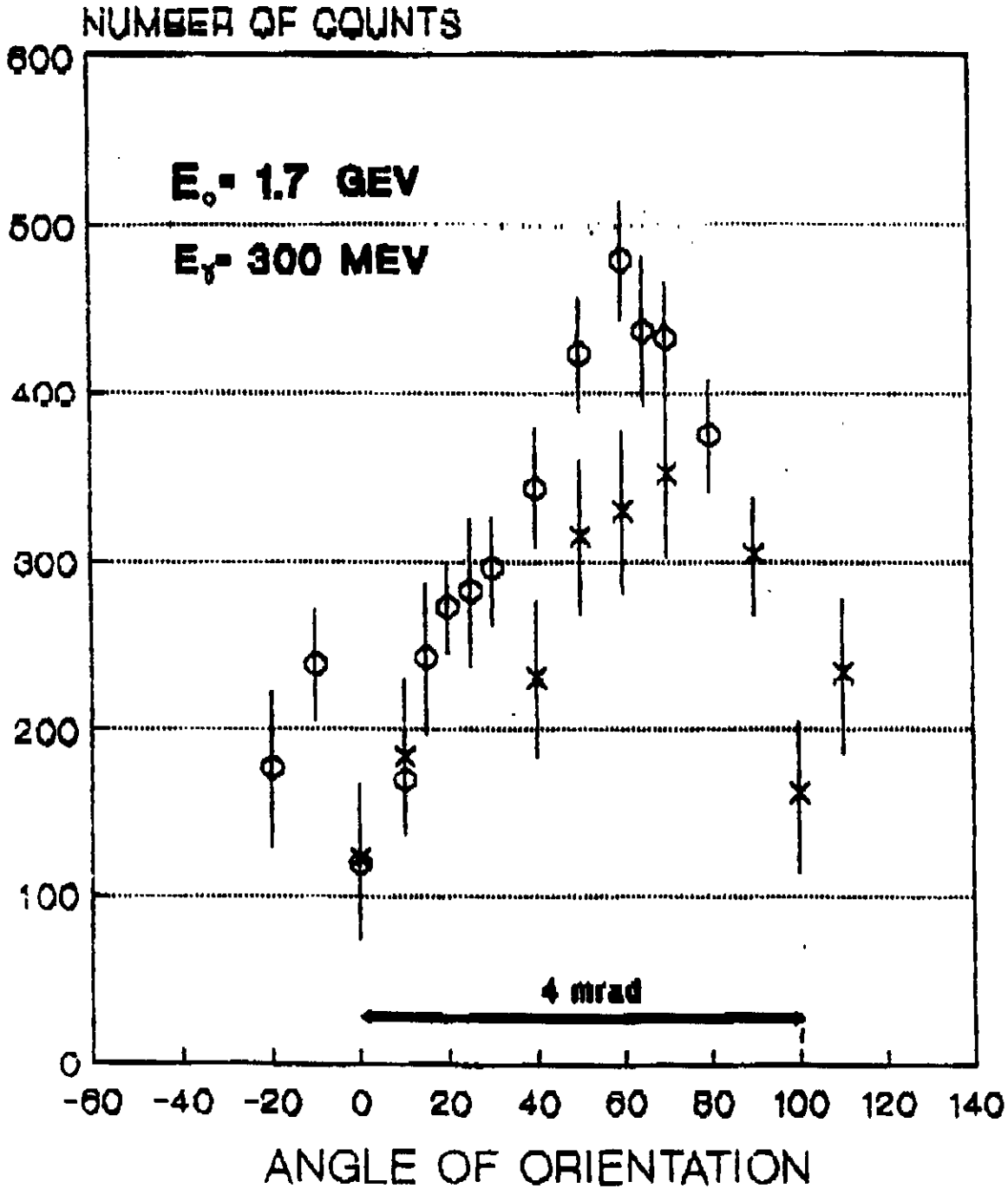

Fig.1. Orientation dependencies of proton yields from reaction photodisintegration of the deuteron. ϕ ($\nparallel$) - polarisation vector of

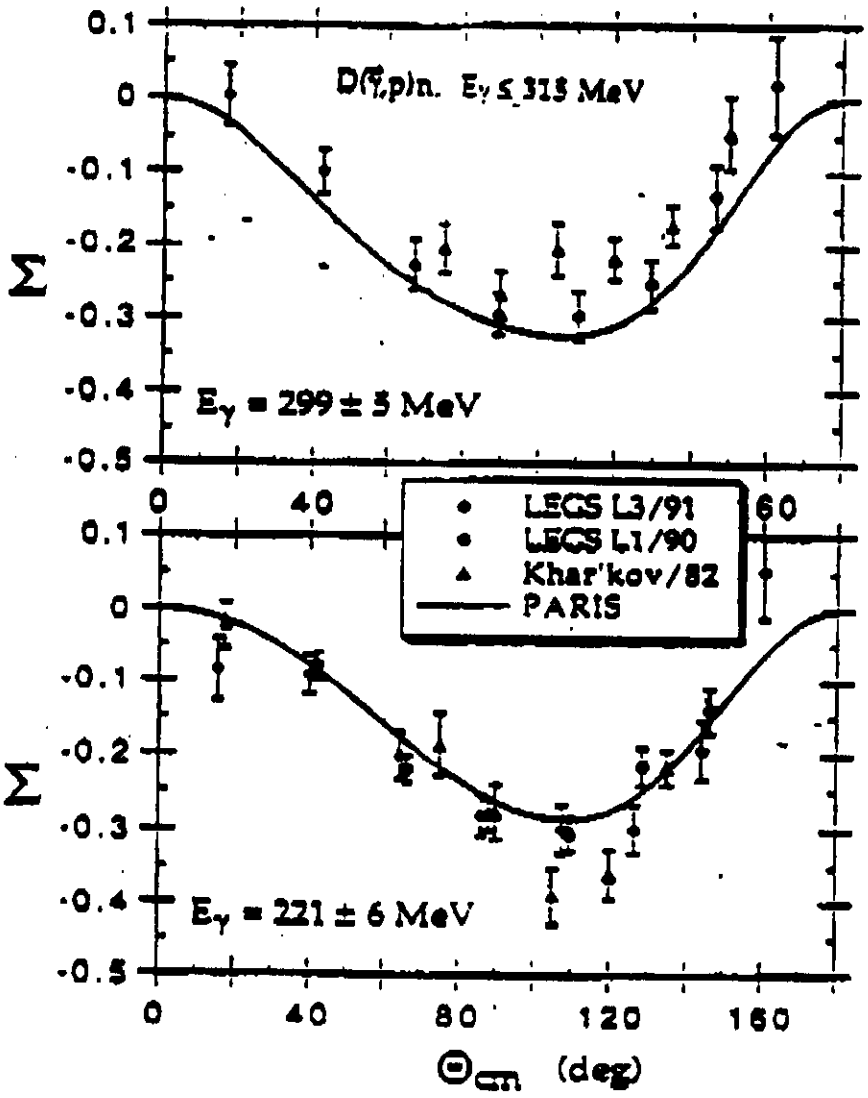

Fig. 12a The comparison between data from experiments TRIUF /19/ and Kharkov for the deuteron photodisintegration / 15 /

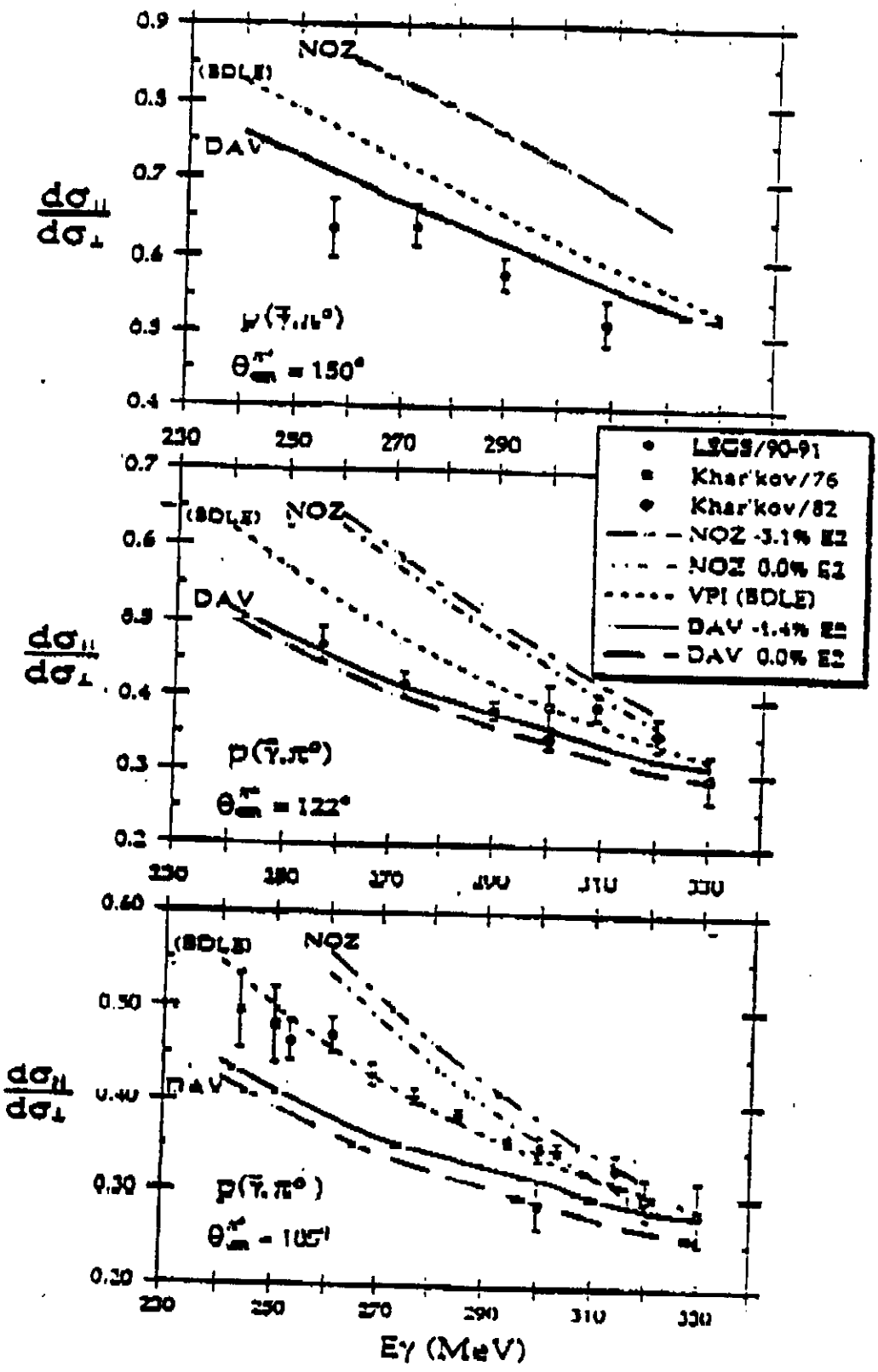

Fig.12b. The same for π^0 photoproduction / 20,21/